

# Structural Studies of Lipopolysaccharide-defective Mutants from *Brucella melitensis* Identify a Core Oligosaccharide Critical in Virulence\*

Received for publication, November 4, 2015, and in revised form, February 10, 2016. Published, JBC Papers in Press, February 11, 2016, DOI 10.1074/jbc.M115.701540

 Carolina Fontana<sup>‡</sup>, Raquel Conde-Álvarez<sup>§</sup>, Jonas Ståhle<sup>‡</sup>, Otto Holst<sup>¶</sup>, Maite Iriarte<sup>§</sup>, Yun Zhao<sup>||</sup>,  
 Vilma Arce-Gorvel<sup>||\*\*††</sup>, Seán Hanniffy<sup>||\*\*††</sup>, Jean-Pierre Gorvel<sup>||\*\*††</sup>, Ignacio Moriyón<sup>§</sup>, and Göran Widmalm<sup>‡#1</sup>

 From the <sup>‡</sup>Department of Organic Chemistry, Arrhenius Laboratory, Stockholm University, S-106 91 Stockholm, Sweden, the <sup>§</sup>Instituto de Salud Tropical, Instituto de Investigación Sanitaria de Navarra, and Departamento de Microbiología y Parasitología, Universidad de Navarra, c/Irunlarrea 1, 31008 Pamplona, Spain, the <sup>¶</sup>Division of Structural Biochemistry, Leibniz-Center for Medicine and Biosciences, Priority Area Asthma and Allergy, Research Center Borstel, Airway Research Center North, Member of the German Center for Lung Research, D-23845 Borstel, Germany, the <sup>||</sup>Centre d'Immunologie de Marseille-Luminy Aix-Marseille University, UM2 Marseille, France, <sup>\*\*</sup>INSERM, U1104 Marseille, France, and <sup>††</sup>CNRS, UMR7280 Marseille, France

The structures of the lipooligosaccharides from *Brucella melitensis* mutants affected in the WbkD and ManB<sub>core</sub> proteins have been fully characterized using NMR spectroscopy. The results revealed that disruption of *wbkD* gives rise to a rough lipopolysaccharide (R-LPS) with a complete core structure ( $\beta$ -D-Glcp-(1→4)- $\alpha$ -Kdop-(2→4)[ $\beta$ -D-GlcpN-(1→6)- $\beta$ -D-GlcpN-(1→4)[ $\beta$ -D-GlcpN-(1→6)]- $\beta$ -D-GlcpN-(1→3)- $\alpha$ -D-Manp-(1→5)]- $\alpha$ -Kdop-(2→6)- $\beta$ -D-GlcpN3N4P-(1→6)- $\alpha$ -D-GlcpN3N1P), in addition to components lacking one of the terminal  $\beta$ -D-GlcpN and/or the  $\beta$ -D-Glcp residues (48 and 17%, respectively). These structures were identical to those of the R-LPS from *B. melitensis* EP, a strain simultaneously expressing both smooth and R-LPS, also studied herein. In contrast, disruption of *manB<sub>core</sub>* gives rise to a deep-rough pentasaccharide core ( $\beta$ -D-Glcp-(1→4)- $\alpha$ -Kdop-(2→4)- $\alpha$ -Kdop-(2→6)- $\beta$ -D-GlcpN3N4P-(1→6)- $\alpha$ -D-GlcpN3N1P) as the major component (63%), as well as a minor tetrasaccharide component lacking the terminal  $\beta$ -D-Glcp residue (37%). These results are in agreement with the predicted functions of the WbkD (glycosyltransferase involved in the biosynthesis of the O-antigen) and ManB<sub>core</sub> proteins (phosphomannomutase involved in the biosynthesis of a mannosyl precursor needed for the biosynthesis of the core and O-antigen). We also report that deletion of *B. melitensis wadC* removes the core oligosaccharide branch not linked to the O-antigen causing an increase in overall negative charge of the remaining LPS inner section. This is in agreement with the mannosyltransferase role predicted for WadC and the lack of GlcpN residues in the defective core oligosaccharide. Despite carrying the O-antigen essential in *B. melitensis* virulence, the core deficiency in the *wadC* mutant structure resulted in a more efficient detection by innate immunity and attenuation, proving the role of the  $\beta$ -

D-GlcpN-(1→6)- $\beta$ -D-GlcpN-(1→4)[ $\beta$ -D-GlcpN-(1→6)]- $\beta$ -D-GlcpN-(1→3)- $\alpha$ -D-Manp-(1→5) structure in virulence.

*Brucella* is a genus of Gram-negative facultative intracellular coccobacilli that causes brucellosis in humans and animals. Although its true extent is not known and the disease is largely unreported (1), it has been estimated that there are half a million new cases every year, most of them located in the poorest rural areas of the world (2). Humans can acquire brucellosis by ingestion of unpasteurized milk from infected animals or by contact with their secretions, but generally they are not themselves a source of contagion. The species within this genus were originally differentiated on the basis of their primary host preferences, with *Brucella melitensis* (sheep and goat), *Brucella suis* (pig), and *Brucella abortus* (cattle) being the most common in domestic livestock. Epidemiological evidence shows that, among them, *B. melitensis* is the most virulent species for humans (3).

The lipopolysaccharides (LPS) of Gram-negative bacteria are exposed on the cell surface, and three different regions with different chemical and biological properties can be identified as follows: the lipid A, the core oligosaccharides, and the polysaccharide, which in most cases represents the O-specific polysaccharide (O-PS,<sup>2</sup> O-antigen) (4, 5). The LPS of *Brucella* shows very low endotoxicity, which illustrates poor detection by innate immunity. Thus, it is considered one of the virulence factors that allow the pathogen to escape early detection by the host immune system (6, 7). Whereas this characteristic is related to the structure of the lipid A and core oligosaccharide of LPS, the O-PS (8, 9) also plays a major role in virulence, because it has been repeatedly observed that mutants lacking the O-PS (*i.e.* producing a rough (R) type LPS, also termed lipooligosaccharide (LOS)) are attenuated (10). *Brucella* strains with R-LPS are often caused by spontaneous mutations (11–13)

\* This work was supported by grants from the Swedish Research Council, the Knut and Alice Wallenberg Foundation, and Ministerio de Economía y Competitividad Grants AGL2011-30453-C04 and AGL2014-58795-C4-1-R; the research that led to these results received funding from the European Commission's Seventh Framework Programme FP7/2007-2013 under Grant Agreement 215536. The authors declare that they have no conflicts of interest with the contents of this article.

✂ Author's Choice—Final version free via Creative Commons CC-BY license.  
<sup>1</sup> To whom the correspondence should be addressed. E-mail: goran.widmalm@su.se.

<sup>2</sup> The abbreviations used are: O-PS, O-specific polysaccharide; LOS, lipooligosaccharide; R-LPS, rough lipopolysaccharide; BMDC, bone marrow-derived dendritic cell; PE, phycoerythrin; Kdo, 3-deoxy-D-manno-oct-2-ulosonic acid; HSQC, heteronuclear single quantum coherence; HMBC, heteronuclear multiple-bond correlation; HR-MS, high resolution mass spectrometry.

## *Brucella melitensis* Rough LPS

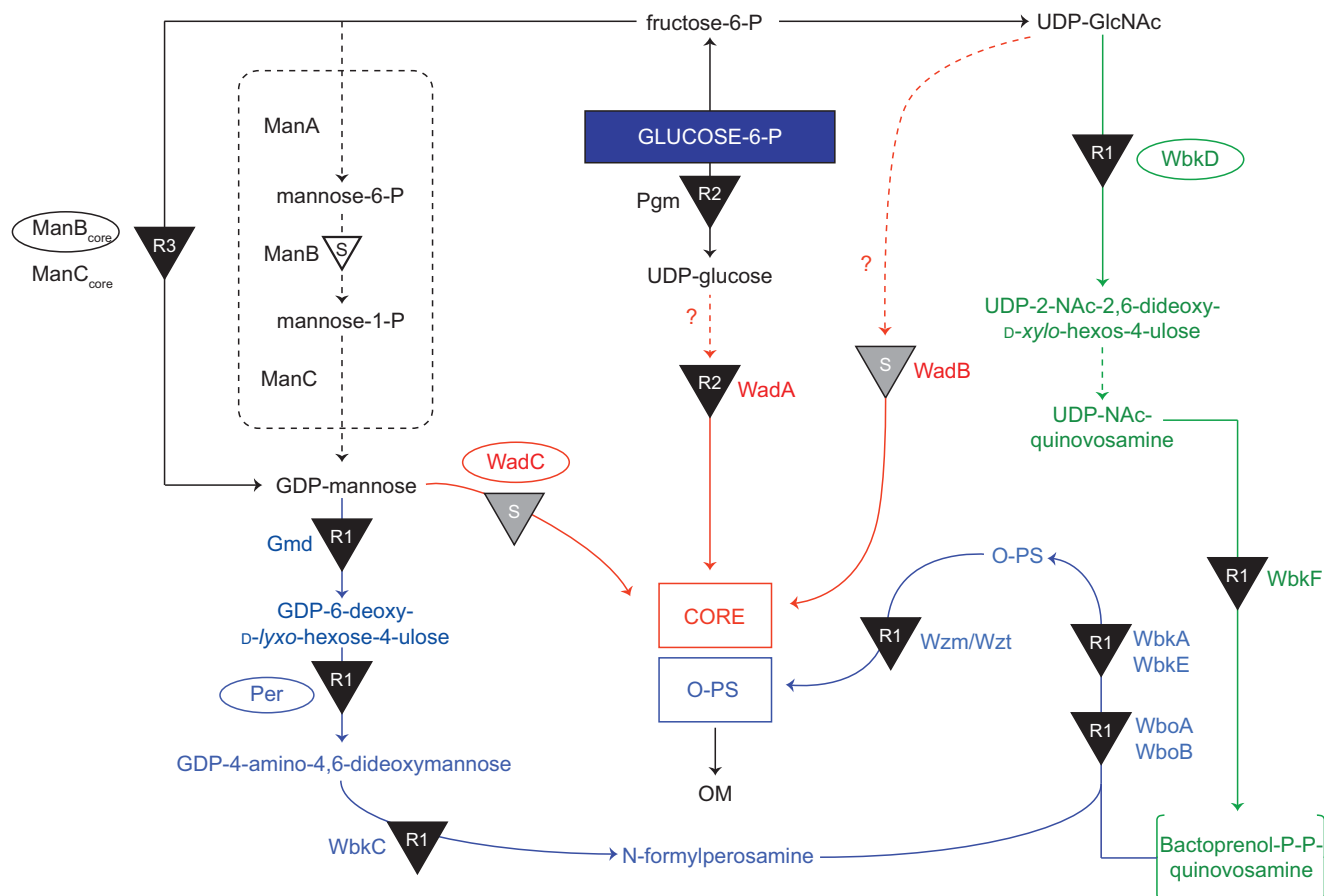


**FIGURE 1. Proposed pathways involved in the biosynthesis of the S-LPS of *B. melitensis*.** Overview of the pathways involved in the biosynthesis of the S-LPS of *B. melitensis* (adapted from Ref. 10). The steps leading to *N*-formylperosamine synthesis and to its polymerization are indicated in blue, and those leading to bactoprenol priming for *N*-formylperosamine polymerization are depicted in green. Subsequently, the O-PS is translocated to the periplasm by the Wzm/Wzt ABC transporter (also in blue) and ligated to the core oligosaccharide that results from the pathways marked in red. The LPS phenotypes obtained by disrupting the different steps (indicated by black triangles) are annotated (R1, R2, or R3). A white-filled triangle (GDP-mannose pathway) indicates a mutation that does not generate an R phenotype, and gray triangles marked with S (middle) indicate a mutation that, while blocking the synthesis of a core lateral branch, does not prevent O-PS linkage to the core. Enzymes disrupted in this study (WadC, Per, WbkD, and ManB<sub>core</sub>) are indicated with an ellipse.

and can also be due to mutation in genes encoding proteins involved in the biosynthesis of the monosaccharide components of the O-PS, its polymerization or transport, or the core oligosaccharide. In a previous report, the genes involved in the biosynthesis of the LPS of *B. melitensis* were screened, and several mutants affected in the biosynthesis of both the core oligosaccharide or O-PS were obtained (10). To assign mutations to the biosynthetic pathways, the mutants were classified as R1 (complete core), R2 (defective core), and R3 (deep R core), respectively, according to the decrease in their LPS apparent molecular mass (10). For instance, mutations in *wbkD*, *wadA*, and *manB<sub>core</sub>* gave rise to R1, R2, and R3 LPS core glycoforms, respectively (10). Based on sequence homology comparisons, *wbkD* was proposed to code for a putative epimerase/dehydratase involved in the biosynthesis of quinovosamine, the monosaccharide located at the reducing end of the O-PS (10, 14, 15). In contrast, *wadA* was proposed to encode a glycosyltransferase involved in the biosynthesis of the core, whereas *manB<sub>core</sub>* was proposed to encode a phosphomannomutase involved in the biosynthesis of GDP-mannose, used as a precursor in the synthesis of both the core oligosaccharide and the perosamine residues found in the O-PS (10, 16). Moreover, it was shown in later works that deletion of genes encoding glycosyltransferases

*wadB* and *wadC* creates severe but uncharacterized defects in the core without affecting the section linked to the O-PS. Remarkably, *B. abortus wadC* mutants are attenuated despite carrying an intact O-PS (17). An overview of the proposed pathways involved in the biosynthesis of the smooth LPS of *B. melitensis* is shown in Fig. 1.

In this study, we describe the structural elucidation of the LOS from *B. melitensis* strain EP, a spontaneous mutant producing O-PS and increased amounts of LOS (18), Bm\_ *wbkD* and Bm\_ *manB<sub>core</sub>*, two mutants in *wbkD* and *manB<sub>core</sub>*, disrupted in the corresponding biosynthetic steps that produce R1 and R3 LOS, respectively (Table 1 and Fig. 1). We also report that deletion of *B. melitensis wadC* removes the core oligosaccharide section not linked to the O-PS. We furthermore show that, despite carrying the O-PS essential in virulence, the lack of this core section results in a marked change in bacterial surface physicochemical properties, a more efficient detection by innate immunity, and attenuation in both cellular and animal models.

### Experimental Procedures

**Bacterial Strains**—*B. melitensis* 16M (biovar 1 reference strain) and *B. melitensis* H38 are wild type virulent strains com-

**TABLE 1**  
**B. melitensis LPS mutants used in the present work**

Name	Parental strain	Gene (ORF)	Role (annotation)	LPS phenotype	Refs.
Bm_ <i>manB</i> <sub>core</sub>	H38	<i>manB</i> <sub>core</sub> (BMEI10899)	Core synthesis (phosphomannomutase)	R3	10
Bm_ <i>wbkD</i>	H38	<i>wbkD</i> (BMEI1427)	O-PS synthesis (epimerase/dehydratase)	R1	10
Bm_ <i>per</i>	16M	<i>per</i> (BMEI1414)	O-PS synthesis (perosamine synthetase)	R1	10, 46, 47
Bm_ <i>wadC</i>	16M	<i>wadC</i> (BMEI0509)	Core synthesis (glycosyltransferase)	S	This work
Bm_ <i>wadC</i> <sub>per</sub>	16M	<i>wadC</i> (BMEI0509)/ <i>per</i> (BMEI1414)	Core and O-PS synthesis	R3	This work

monly used in virulence studies that are identical with regard to LPS genes (10). *B. melitensis* EP (henceforth BmEPR) is a strain that, although virulent and able to synthesize O-polysaccharides, produces comparatively large proportions of R-LPS (18) and is thus suitable to obtain R-LPS in large amounts for chemical analyses. Mutants with defects in LPS genes (Table 1 and Fig. 1) were obtained, characterized, and stored according to the procedures described previously (10, 17).

**Growth of Bacteria and Isolation of the LOS**—Bacteria were propagated in tryptic soy broth either in a Biostat fermentor (BmEPR, Bm\_ *wbkD*, and Bm\_ *manB*<sub>core</sub>) or in 2-liter flasks (Bm\_ *wadC* and Bm\_ *wadC*<sub>per</sub>) on an orbital shaker in a BSL3 facility. After 36 h of incubation, bacteria were inactivated with phenol, harvested by tangential flow filtration, and washed twice with saline (19). For LOS extraction (BmEPR, Bm\_ *wbkD*, Bm\_ *manB*<sub>core</sub>, and Bm\_ *wadC*<sub>per</sub>), bacteria were first acetone-dried and then extracted following the phenol/chloroform/light petroleum method (20), and the overall defect (R1, R2, and R3) in the R-LPS was confirmed by SDS-PAGE and silver staining and absence of reactivity with O-PS specific monoclonal antibodies (10). The LPS of Bm\_ *wadC* was obtained from the phenol phase of a water/phenol extract and further purified as described before (21).

**Compositional Analyses**—Quantitative analyses of sugars, organic bound phosphate, and fatty acids were performed as described previously (22).

**Preparation of the Deacylated Oligosaccharides**—The LOS from the different *B. melitensis* mutants were O-deacylated using hydrazine, followed by N-deacylation with hot KOH (23) and purified by high performance anion-exchange chromatography.

**Mass Spectrometry**—Electrospray ionization high resolution mass spectra (ESI-HR-MS) were recorded in negative ion mode using a MicrOTOF<sup>TM</sup> mass spectrometer (Bruker Daltonics). Nitrogen was used as the collision gas.

**NMR Spectroscopy**—The deacylated LOSs of BmEPR (3.8 mg), Bm\_ *wbkD* (2.4 mg), and Bm\_ *manB*<sub>core</sub> (3.4 mg) were deuterium-exchanged by freeze-drying three times from 99.9% D<sub>2</sub>O and examined as a solution of 99.96% D<sub>2</sub>O (0.55 ml) at pD 8 and 25 °C. Chemical shifts are reported in parts/million using internal sodium 3-trimethylsilyl-(2,2,3,3-<sup>2</sup>H<sub>4</sub>)-propanoate ( $\delta_{\text{H}}$  0.00), external 1,4-dioxane in D<sub>2</sub>O ( $\delta_{\text{C}}$  67.40), or external 2% phosphoric acid in D<sub>2</sub>O ( $\delta_{\text{P}}$  0.00) as references.

The diffusion-filtered <sup>1</sup>H NMR spectrum of the deacylated LOS from Bm\_ *manB*<sub>core</sub> was recorded on a Bruker Avance 500 MHz spectrometer equipped with a 5-mm Z-gradient (53.0 G·cm<sup>-1</sup>) TCI (<sup>1</sup>H/<sup>13</sup>C/<sup>15</sup>N) CryoProbe using the one-dimensional stimulated spin-echo pulse sequence with bipolar gradients and LED (ledbpgp2s1d) (24). Diffusion-encoded sinusoidal

gradients pulses ( $\delta/2$ ) of 1.8 ms and a strength of 70% of the maximum were used; the diffusion time was set to 100 ms. The one-dimensional diffusion-filtered <sup>1</sup>H NMR spectra of the deacylated LOS from BmEPR and Bm\_ *wbkD* were recorded on a Bruker Avance III 700 MHz spectrometer equipped with a 5-mm Z-gradient (53.0 G·cm<sup>-1</sup>) TCI (<sup>1</sup>H/<sup>13</sup>C/<sup>15</sup>N) CryoProbe, using the same pulse sequence as described above and diffusion-encoded smoothed square-shape gradient pulses ( $\delta/2$ ) of 1.8 ms and a strength of 50% of the maximum; the diffusion time was set to 120 ms.

<sup>1</sup>H and <sup>13</sup>C NMR chemical shifts assignments of the three LOS materials referred to in the preceding paragraph were obtained from experiments recorded at a magnetic field strength of 16.4 tesla. <sup>1</sup>H chemical shift assignments were obtained using <sup>1</sup>H, <sup>1</sup>H TOCSY experiments (25) employing the States-TPPI method, an MLEV-17 spin-lock of 10 kHz, and different mixing times (between 20 and 100 ms). To identify correlations from possible impurities of lower molecular mass than the deacylated LOSs from Bm\_ *manB*<sub>core</sub>, a diffusion-filtered <sup>1</sup>H, <sup>1</sup>H TOCSY experiment ( $\tau_m = 100$  ms) was acquired employing the pulse sequence “ledbpgpml2s2d” from the standard Bruker library; diffusion-encoded smoothed square-shape gradient pulses ( $\delta/2$ ) of 1.8 ms and strength of 70% of the maximum were used and a diffusion time of 150 ms.

<sup>13</sup>C NMR chemical shifts were obtained from the respective <sup>13</sup>C spectra, and the assignments were carried out using multiplicity-edited <sup>1</sup>H, <sup>13</sup>C HSQC experiments (26) employing the echo/anti-echo method. Adiabatic pulses (27, 28) were used for <sup>13</sup>C inversion (smoothed CHIRP, 20%, 80 kHz, 500  $\mu$ s, Q = 5.0) (29) and refocusing (composite smoothed CHIRP, 80 kHz, 2.0 ms). The <sup>1</sup>H, <sup>13</sup>C-H2BC experiments (30) were recorded with a constant-time delay of 33 ms, and the <sup>1</sup>H, <sup>13</sup>C HSQC TOCSY experiments were acquired using an MLEV-17 spin-lock of 10 kHz employing mixing times ranging from 20 to 100 ms.

For assignments of inter-residue correlations, <sup>1</sup>H, <sup>1</sup>H NOESY and <sup>1</sup>H, <sup>13</sup>C heteronuclear multiple-bond correlation (HMBC) experiments were utilized. The gradient-selected <sup>1</sup>H, <sup>1</sup>H NOESY experiments (31) were recorded with a mixing time of 100 ms, whereas the gradient-selected <sup>1</sup>H, <sup>13</sup>C HMBC experiments (32) were carried out with an evolution time of 65 ms. Band-selective constant-time <sup>1</sup>H, <sup>13</sup>C HMBC experiments (33) with 2-fold low pass J-filters (hmbcctetgpl2nd) were also employed to improve spectral resolution in the anomeric region. The experiments were recorded over a spectral region of 5.4  $\times$  9.0 ppm with 2048  $\times$  256 data points, using an 80-ms delay for evolution of the long range couplings. A selective <sup>13</sup>C excitation pulse (Q3 gaussian cascade) of 2.5 ms was applied at the center of the anomeric region.

## *Brucella melitensis* Rough LPS

$^{31}\text{P}$ -based NMR experiments were obtained on a Bruker Avance III 600 MHz spectrometer equipped with a 5-mm Z-gradient ( $55.7\text{ G}\cdot\text{cm}^{-1}$ ) inverse TXI ( $^1\text{H}/^{13}\text{C}/^{31}\text{P}$ ) probe. The one-dimensional  $^1\text{H}$ -decoupled  $^{31}\text{P}$  NMR spectra were recorded with a spectral width of 396 ppm, and the  $^{31}\text{P}$  chemical shifts assignments were obtained from gradient selected  $^1\text{H},^{31}\text{P}$  HMBC (32, 34) and  $^1\text{H},^{31}\text{P}$ -hetero TOCSY experiments (35). The  $^1\text{H},^{31}\text{P}$  HMBC spectra were recorded with an evolution time of 100 ms. The  $^1\text{H},^{31}\text{P}$ -hetero TOCSY experiments were carried out with mixing times of 23 and 46 ms, using a DIPSI2 mixing sequence set at 5 kHz on both channels or with a mixing time of 92 ms using a DIPSI2 mixing sequence set at 2.5 kHz.

Additionally, NMR experiments selected from those described above were carried out on deacylated tetra- and pentasaccharides from Bm\_wadC\_per on 0.28 and 0.26 mg, respectively, in  $\text{D}_2\text{O}$  (0.55 ml) at pD 7, a temperature of  $15^\circ\text{C}$ , and a  $^1\text{H}$  frequency of 500 MHz.

**$\zeta$  Potential**—The surface charge density was measured as the electrophoretically effective potential ( $\zeta$  potential,  $\zeta_{\text{sm}}$ ) as described previously (10). For this, bacteria were grown in tryptic soy broth, inactivated with 0.5% phenol, washed, and resuspended in 1 mM CsCl, 10 mM HEPES (pH 7.2) at an  $A_{600}$  of 0.2. Measurements were performed at  $25^\circ\text{C}$  in a Zetamaster instrument using the PCS 1.27 software (Malvern Instruments Ltd., Malvern, UK).

**Virulence Assays**—Bone marrow cells were isolated from femurs of a 7–8-week-old C57Bl/6 female mice and differentiated into dendritic cells (BMDCs) as described by Inaba *et al.* (36). Infections were performed by centrifuging the bacteria onto the differentiated cells ( $400 \times g$  for 10 min at  $4^\circ\text{C}$ ; bacteria/cell ratio of 20:1 followed by incubation at  $37^\circ\text{C}$  for 30 min under a 5%  $\text{CO}_2$  atmosphere). BMDCs were gently washed with medium to remove extracellular bacteria before incubating in a medium supplemented with  $100\ \mu\text{g}\cdot\text{ml}^{-1}$  gentamicin for 1 h to kill extracellular bacteria. Thereafter, the antibiotic concentration was decreased to  $20\ \mu\text{g}\cdot\text{ml}^{-1}$ . To monitor *Brucella* intracellular survival, BMDCs were lysed with 0.1% (v/v) Triton X-100 in  $\text{H}_2\text{O}$ , and serial dilutions of lysates were rapidly plated onto tryptic soy agar plates to enumerate the colony-forming units (cfu).

Seven-week-old female BALB/c mice (Charles River, Elbeuf, France) were kept in cages with water and food *ad libitum* and accommodated under BSL3 biosafety containment 2 weeks before and during the experiments in the facilities of the “CIMA” (registration code ES31 201000132). The animal handling and other procedures were in accordance with the current European (directive 86/609/EEC) and Spanish (RD 53/2013) legislations, supervised by the Animal Welfare Committee of the University of Navarra (CEEA 045/12). Inocula were prepared in sterile 10 mM PBS (pH 6.85), and  $\sim 5 \times 10^4$  cfu in 0.1 ml (the exact dose was assessed retrospectively by plating dilutions of the inocula) were administered intraperitoneally to each mouse. For each strain, 10 mice were inoculated, and the number of cfu in spleen was determined at 2 and 8 weeks after inoculation as described previously (37). The individual data were normalized by logarithmic transformation.

**Flow Cytometry**—To analyze activation and maturation, BMDCs were analyzed for surface expression of classical mat-

uration markers at 24 h post-treatment with the different LPS variants. Cells were labeled with fluorochrome-conjugated antibodies specific for mouse CD11c:PE-Cy7 (clone N418), IA-IE:PE (MHC class II clone M5/114.15.2) (PE), CD86:FITC (Clone GL-1), CD40:AlexaFluor 647 (clone 3/23), and CD80:PE-Cy5 (clone 16-10A1), all from BioLegend. Labeled cells were then subjected to multicolor cytometry using an LSR II UV spectrophotometer (BD Biosciences), and the data were analyzed using FlowJo software by first gating on the  $\text{CD11c}^+$  population (100,000 events) prior to quantifying expression of receptors. Cells were stimulated with  $10\ \mu\text{g}\cdot\text{ml}^{-1}$  of LPS purified from the *B. melitensis* wild type or Bm\_wadC mutant strain or with *Escherichia coli* LPS (O55:B5) as a positive control.

**Cytokine Measurement**—Murine IL-6, IL-12p70, and TNF- $\alpha$  were quantified in culture supernatants of stimulated BMDC by sandwich enzyme-linked immunosorbent assays (ELISA) according to the manufacturer's protocol (eBioscience).

## Results

### Compositional Analyses

The analysis of sugars, fatty acids, and organic bound phosphate (P) of the LOS from mutants Bm\_manB\_core, Bm\_wbkD, and BmEPR revealed the presence (in  $\text{nmol}\cdot\text{mg}^{-1}$  LOS) of Glc (164/176/110, respectively), Kdo (714/536/572), GlcN (53/637/680), P (1017/782/659), 12:0(3-OH) (88/96/138), 16:0(3-OH) (316/258/283), 16:0 (349/286/188), 18:0 (100/89/102), cyclo19:0 (55/154/105), and 28:0(27-OH)/28:0(27-oxo) (161/99/90). GlcN3N was not quantified. Mannose was present in trace amounts in the LOS from BmEPR but was lacking in the other two LOSs, because it was not present at all in Bm\_manB\_core and was not released under the acidic hydrolysis conditions used due to its substitution by GlcN (compare structures below).

### Mass Spectrometry

**HRMS of the LOS from Bm\_manB\_core**—The two sets of single negatively charged pseudo-molecular ions observed in the high resolution mass spectrum of the deacylated LOS from Bm\_manB\_core (Fig. 2A) are consistent with the presence of two different oligosaccharides. The ions at  $m/z$  1099.3 and 937.2 correspond to species formed through the loss of a proton. The former ion is in agreement with the presence of a pentasaccharide composed of one hexose (Hex), two Kdo, two diamino-hexoses (HexNN), and two phosphate groups (P), whereas the latter indicate the presence of a tetrasaccharide composed of two Kdo residues, two diamino-hexoses, and two phosphate groups (see Table 2). Different singly negatively charged sodium adducts of the pentasaccharide are observed at  $m/z$  1121.3, 1143.2, and 1165.2, whereas those of the tetrasaccharide can be found at  $m/z$  959.2, 981.2, and 1003.2.

**HRMS of the LOS from Bm\_wbkD**—The mass spectrum of the deacylated core oligosaccharide from Bm\_wbkD (Fig. 2B) is also consistent with the presence of two major oligosaccharides, which produce the doubly negatively charged ions at  $m/z$  952.3 and 871.8 through the loss of two protons each. The ion with higher  $m/z$  value corresponds to a decasaccharide composed of two Hex, four hexosamines (HexN), two Kdo, two HexNN, and two phosphate groups (see Table 2); the different doubly charged sodium adducts of this oligosaccharide appear

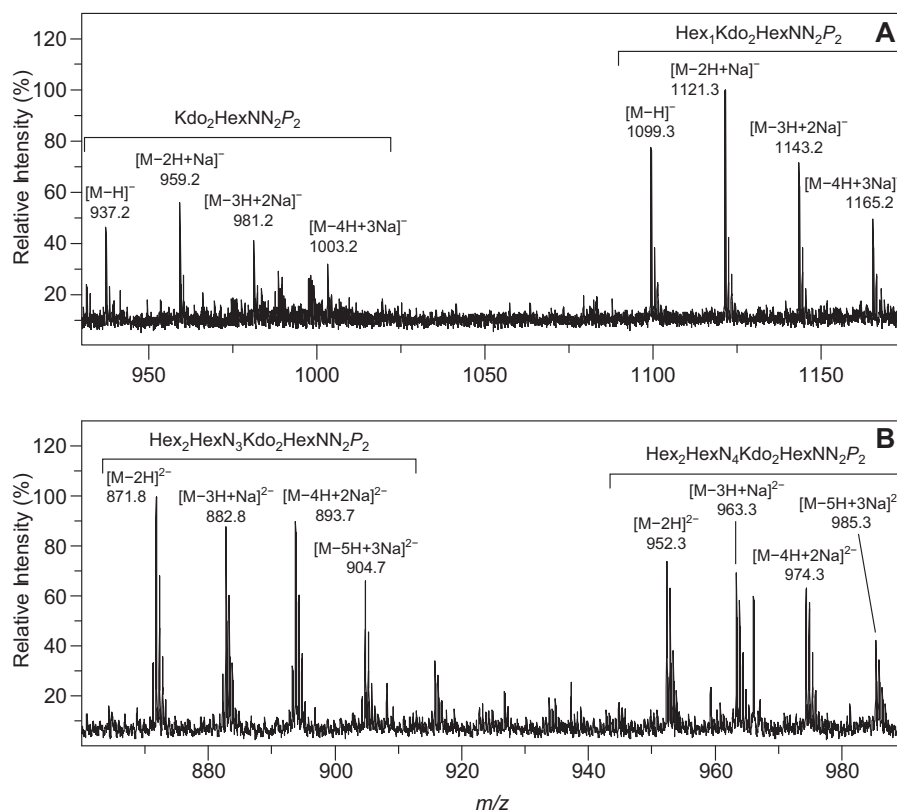


FIGURE 2. **Mass spectra of deacylated LOS.** Selected regions of the high resolution mass spectra of the deacylated core oligosaccharides of *Bm\_manB<sub>core</sub>* (A) and *Bm\_wbkD* (B) recorded in negative ion mode. The clusters of pseudo-molecular ions originating from the two major components of each sample are annotated (see Table 2). Note that the peaks observed in A and B correspond to singly and doubly negatively charged ion species, respectively.

**TABLE 2**

**HR-MS data (negative ion mode) and proposed compositions of the LPS from *Bm\_manB<sub>core</sub>* and *Bm\_wbkD***

Summary of the diagnostic pseudo-molecular ions observed in the high resolution mass spectra of the deacylated LOS from *Bm\_manB<sub>core</sub>* and *Bm\_wbkD* and the proposed composition of the two main components present in each sample. The components are abbreviated as follow: Hex (hexoses), HexN (hexosamine), HexNN (diaminohexose), and P (phosphate group).

Mutant name	Pseudo-molecular ions ( <i>m/z</i> )			Molecular formula	Proposed composition (exact molecular mass)
	Observed	Calculated	Annotation		
<i>Bm_manB<sub>core</sub></i> (Fig. 2A)	1099.2680	1099.2750	[M - H] <sup>-</sup>	C <sub>34</sub> H <sub>61</sub> N <sub>4</sub> O <sub>32</sub> P <sub>2</sub> <sup>-</sup>	Hex <sub>1</sub> Kdo <sub>2</sub> HexNN <sub>2</sub> P <sub>2</sub> (1100.2822)
	1121.2520	1121.2569	[M - 2H + Na] <sup>-</sup>	C <sub>34</sub> H <sub>60</sub> N <sub>4</sub> O <sub>32</sub> P <sub>2</sub> Na <sup>-</sup>	
	1143.2344	1143.2389	[M - 3H + 2Na] <sup>-</sup>	C <sub>34</sub> H <sub>59</sub> N <sub>4</sub> O <sub>32</sub> P <sub>2</sub> Na <sub>2</sub> <sup>-</sup>	
	1165.2195	1165.2208	[M - 4H + 3Na] <sup>-</sup>	C <sub>34</sub> H <sub>58</sub> N <sub>4</sub> O <sub>32</sub> P <sub>2</sub> Na <sub>3</sub> <sup>-</sup>	
	937.2173	937.2221	[M - H] <sup>-</sup>	C <sub>28</sub> H <sub>51</sub> N <sub>4</sub> O <sub>27</sub> P <sub>2</sub> <sup>-</sup>	Kdo <sub>2</sub> HexNN <sub>2</sub> P <sub>2</sub> (938.2294)
	959.1989	959.2041	[M - 2H + Na] <sup>-</sup>	C <sub>28</sub> H <sub>50</sub> N <sub>4</sub> O <sub>27</sub> P <sub>2</sub> Na <sup>-</sup>	
	981.1896	981.1860	[M - 3H + 2Na] <sup>-</sup>	C <sub>28</sub> H <sub>49</sub> N <sub>4</sub> O <sub>27</sub> P <sub>2</sub> Na <sub>2</sub> <sup>-</sup>	
<i>Bm_wbkD</i> (Fig. 2B)	1003.1579	1003.1680	[M - 4H + 3Na] <sup>-</sup>	C <sub>28</sub> H <sub>48</sub> N <sub>4</sub> O <sub>27</sub> P <sub>2</sub> Na <sub>3</sub> <sup>-</sup>	Hex <sub>2</sub> HexN <sub>4</sub> Kdo <sub>2</sub> HexNN <sub>2</sub> P <sub>2</sub> (1906.6103)
	952.2962	952.2978	[M - 2H] <sup>2-</sup>	C <sub>64</sub> H <sub>114</sub> N <sub>8</sub> O <sub>53</sub> P <sub>2</sub> <sup>2-</sup>	
	963.2803	963.2888	[M - 3H + Na] <sup>2-</sup>	C <sub>64</sub> H <sub>113</sub> N <sub>8</sub> O <sub>53</sub> P <sub>2</sub> Na <sup>2-</sup>	
	974.2724	974.2798	[M - 4H + 2Na] <sup>2-</sup>	C <sub>64</sub> H <sub>112</sub> N <sub>8</sub> O <sub>53</sub> P <sub>2</sub> Na <sub>2</sub> <sup>2-</sup>	
	985.2674	985.2708	[M - 5H + 3Na] <sup>2-</sup>	C <sub>64</sub> H <sub>111</sub> N <sub>8</sub> O <sub>53</sub> P <sub>2</sub> Na <sub>3</sub> <sup>2-</sup>	
	871.7581	871.7635	[M - 2H] <sup>2-</sup>	C <sub>58</sub> H <sub>103</sub> N <sub>7</sub> O <sub>49</sub> P <sub>2</sub> <sup>2-</sup>	Hex <sub>2</sub> HexN <sub>3</sub> Kdo <sub>2</sub> HexNN <sub>2</sub> P <sub>2</sub> (1745.5415)
	882.7532	882.7544	[M - 3H + Na] <sup>2-</sup>	C <sub>58</sub> H <sub>102</sub> N <sub>7</sub> O <sub>49</sub> P <sub>2</sub> Na <sup>2-</sup>	
	893.7469	893.7454	[M - 4H + 2Na] <sup>2-</sup>	C <sub>58</sub> H <sub>101</sub> N <sub>7</sub> O <sub>49</sub> P <sub>2</sub> Na <sub>2</sub> <sup>2-</sup>	
	904.7361	904.7364	[M - 5H + 3Na] <sup>2-</sup>	C <sub>58</sub> H <sub>100</sub> N <sub>7</sub> O <sub>49</sub> P <sub>2</sub> Na <sub>3</sub> <sup>2-</sup>	

at *m/z* 963.3, 974.3, and 985.3. The ion at *m/z* 871.8 corresponds to a nonasaccharide composed of two Hex, three HexN, two Kdo, two HexNN, and two phosphate groups; ions from three different sodium adducts of this compound are present at *m/z* 882.8, 893.7, and 904.7.

**NMR Spectroscopy**

*LOS from Bm\_manB<sub>core</sub>*—In the <sup>1</sup>H NMR spectrum, three resonances corresponding to anomeric protons were identified

as follows: two doublets at 4.577 and 4.632 ppm (<sup>3</sup>J<sub>H1,H2</sub> = 8.1 and 8.0 Hz, respectively) and one doublet of doublets at 5.430 ppm (<sup>3</sup>J<sub>H1,H2</sub> = 3.2 Hz and <sup>3</sup>J<sub>P,H1</sub> = 8.2 Hz). The residues were named A, E, and B, in order of decreasing <sup>1</sup>H chemical shifts (Fig. 3A). Two major resonances were identified in the <sup>31</sup>P NMR spectrum at 2.6 and 3.2 ppm, suggesting the presence of two phosphomonoester groups, one of which is consistent with the splitting of the H1 resonance of residue A. All the protons from H1 to H6 could be traced using <sup>1</sup>H,<sup>1</sup>H TOCSY experi-

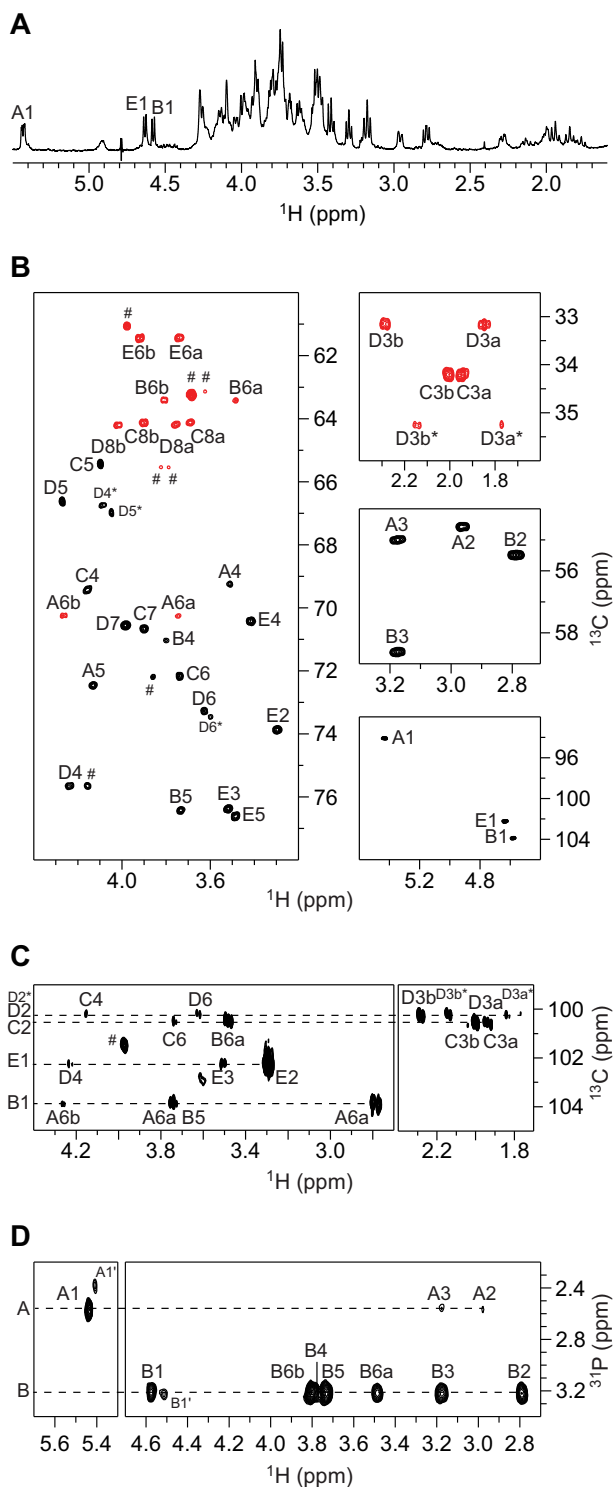


FIGURE 3. NMR spectra of the deacylated LOS from *Bm\_manB<sub>core</sub>*. **A**, selected region of the diffusion-filtered  $^1\text{H}$  NMR spectrum. **B**, selected regions of the multiplicity-edited  $^1\text{H},^{13}\text{C}$  HSQC spectrum showing the anomeric region (right bottom), the region for the nitrogen-bearing carbons (right middle), the region for the 3-deoxy-groups of the Kdo residues (right top), and the region for the ring atoms and those from hydroxymethyl groups (left) in which the cross-peaks from the latter appear in red. **C**, selected region of the  $^1\text{H},^{13}\text{C}$  HMBC spectrum showing intra- and inter-residue correlations from anomeric carbons. **D**, selected region of the  $^1\text{H},^{31}\text{P}$ -hetero TOCSY spectrum ( $\tau_m = 92$  ms) showing correlations from the phosphate groups in residues **A** and **B**. Signals from impurities of lower molecular mass than the LOS oligosaccharides of *B. melitensis* are indicated by the hash symbol.

ments, indicating that these residues have the *gluco*-configuration.  $^{13}\text{C}$  NMR chemical shifts were assigned using multiplicity-edited  $^1\text{H},^{13}\text{C}$  HSQC (Fig. 3B) and  $^1\text{H},^{13}\text{C}$  H2BC experiments. Both C2 and C3 resonances of residues **A** and **B** were found in the region between 54 and 59 ppm (Fig. 3B, right middle), which indicates that these are nitrogen-bearing carbons.  $^1J_{\text{C1,H1}}$  couplings constants were extracted from a coupled  $^1\text{H},^{13}\text{C}$  HSQC spectrum and revealed that residues **B** and **E** are  $\beta$ -linked ( $^1J_{\text{C1,H1}} = 164$  and 163 Hz, respectively), whereas residue **A** is  $\alpha$ -linked ( $^1J_{\text{C1,H1}} = 174$  Hz); thus **A** is  $\alpha$ -D-GlcpN3N, **B** is  $\beta$ -D-GlcpN3N, and residue **E** is  $\beta$ -D-Glcp. In the  $^{13}\text{C}$  NMR spectrum, three anomeric carbons were identified at 100.10, 100.15, and 100.46 ppm and attributed to C2 resonances in three different populations of Kdo residues (**D\***, **D**, and **C**, respectively). In the  $^1\text{H},^{13}\text{C}$  HMBC spectrum, the C2 carbon of each Kdo residue could be correlated to their respective H3 protons via two-bond heteronuclear correlations (Fig. 3C), and the H3 resonances were used as starting points for the assignments of the respective spin systems. The multiplicity-edited  $^1\text{H},^{13}\text{C}$  HSQC spectrum (Fig. 3B, right top) showed cross-peaks of different relative intensities for each of the Kdo residues, which was confirmed by integration of the H3a resonances in the  $^1\text{H}$  NMR spectrum (1.0 H, 0.6 H, and 0.4 H, in residues **C**, **D**, and **D\***, respectively) and indicated the presence of two different oligosaccharide components.  $^1\text{H}$  and  $^{13}\text{C}$  chemical shifts assignments are compiled in Table 3. The  $\alpha$ -configuration of the anomeric center of the Kdo residues was established by comparison of the  $^{13}\text{C}$  chemical shifts of the **D\*-C** moiety with those of the same moiety found in a tetrasaccharide with similar structure, previously reported in the literature (38). Inter-residue correlations were observed in the  $^1\text{H},^{13}\text{C}$  HMBC spectrum from all the anomeric carbons to the respective protons at the substitution positions (Fig. 3C), as well as from the anomeric protons (in residues **E** and **B**) to the respective glycosyloxylated carbons in the next residue (Table 3). These results are in agreement with a major ( $\sim 63\%$ ) pentasaccharide component (**E-D-C-B-A**) in which a Kdo residue (**D**) is 4-substituted with a Glc residue (**E**) and a minor ( $\sim 37\%$ ) tetrasaccharide component (**D\*-C-B-A**) in which the Glc residue is absent, and consequently the corresponding Kdo residue (**D\***) is non-substituted. The percentages of each component were determined by integration of the C3/H3b cross-peaks of residues **D** and **D\*** in the  $^1\text{H},^{13}\text{C}$  HSQC spectrum. The substitution positions of the phosphomonoester groups were determined using  $^1\text{H},^{31}\text{P}$  HMBC and  $^1\text{H},^{31}\text{P}$ -hetero TOCSY experiments and were found at C1 in residue **A** ( $^3J_{\text{P,H1}} = 8.2$  Hz,  $^2J_{\text{P,C1}} = 5.4$  Hz, and  $^3J_{\text{P,C2}} = 6.1$  Hz) and C4 in residue **B** (Fig. 3D). Three additional resonances of minor intensities were found in the  $^{31}\text{P}$  NMR spectrum at  $\delta_p$  4.0 (t,  $^3J_{\text{P,H}} = 7.0$  Hz), 4.1 (d,  $^3J_{\text{P,H}} = 8.2$  Hz), and 4.4 (t,  $^3J_{\text{P,H}} = 6.8$  Hz) and were attributed to free phosphoethanolamine, glycerol 2-phosphate, and glycerol 3-phosphate, respectively. The  $^1\text{H}$  resonances of these three components could readily be identified in the  $^1\text{H},^{31}\text{P}$  HMBC and  $^1\text{H},^{31}\text{P}$ -hetero TOCSY spectra and correlated to their respective carbons in the multiplicity-edited  $^1\text{H},^{13}\text{C}$  HSQC (denoted with the hash symbol in Fig. 3B, left). The chemical shifts assignments of these three components (phosphoethanolamine, 3.975/61.05 and 3.210/41.48 ppm; glycerol 2-phosphate, 4.155/75.64 and 3.682/62.24 ppm;

**TABLE 3**

**NMR chemical shift assignments of the LOS from *Bm\_manB<sub>core</sub>* and *Bm\_wadC<sub>per</sub>* and inter-residue correlations from <sup>1</sup>H,<sup>13</sup>C HMBC NMR spectra**

The <sup>1</sup>H, <sup>13</sup>C, and <sup>31</sup>P NMR chemical shifts (ppm) of the LOS from *Bm\_manB<sub>core</sub>* were determined at 25 °C and pD 8, whereas the <sup>1</sup>H and <sup>13</sup>C NMR chemical shifts of the tetra- and pentasaccharide from *Bm\_wadC<sub>per</sub>* (OS1 and OS2, respectively) were obtained at 15 °C and pD 7. <sup>3</sup>J<sub>H1,H2</sub> values are given in parentheses and <sup>1</sup>J<sub>C1,H1</sub> values in braces. For residue **A**, <sup>3</sup>J<sub>P,H1</sub> = 8.2 Hz, <sup>2</sup>J<sub>P,C1</sub> = 5.4 Hz, and <sup>3</sup>J<sub>P,C2</sub> = 6.1 Hz. ND means not determined.

Sample/sugar residues		<sup>1</sup> H/ <sup>13</sup> C								<sup>31</sup> P	HMBC correlations (from anomeric atom)
		1	2	3	4	5	6	7	8		
<b><i>Bm_manB<sub>core</sub></i></b>											
→6)-α-D-GlcpN3N1P	A	5.430 (3.2) 94.08 {174}	2.955 54.59	3.171 54.97	3.508 69.27	4.128 72.43	3.742, 4.263 70.23			2.6	
→6)-β-D-GlcpN3N4P-(1→	B	4.577 (8.1) 103.87 {164}	2.786 55.47	3.172 58.60	3.797 71.05	3.730 76.41	3.481, 3.804 63.40			3.2	C6, A H6a/H6b, A
→4)-α-Kdop-(2→	C	175.75	100.46	1.940, 2.002 34.20	4.156 69.45	4.096 65.42	3.738 72.15	3.897 70.65	3.689, 3.899 64.11		H6a, B
→4)-α-Kdop-(2→	D	177.40	100.15	1.846, 2.286 33.13	4.237 75.63	4.270 66.60	3.626 73.25	3.983 70.55	3.754, 4.016 64.16		H4, C
α-Kdop-(2→ (without residue E)	D*	176.66	100.10	1.769, 2.144 35.22	4.086 66.71	4.047 66.95	3.598 73.44	3.983 70.57	~3.754, ~4.016 64.22		H4, C* <sup>(a)</sup>
β-D-Glcp-(1→	E	4.632 (8.0) 102.23 {163}	3.296 73.84	3.521 76.36	3.418 70.39	3.485 76.59	3.737, 3.918 61.40				C4, D H4, D
<b><i>Bm_wadC<sub>per</sub></i> OS1</b>											
→6)-α-D-GlcpN3N1P	A	5.445 94.05	3.031 54.22	3.242 55.14	3.562 68.88	4.143 72.55	3.752, 4.268 70.25				
→6)-β-D-GlcpN3N4P-(1→	B	4.600 104.00	2.812 55.40	3.219 58.66	3.815 70.82	3.739 76.47	3.491, 3.810 63.46				
→4)-α-Kdop-(2→	C	ND	ND	1.946, 1.987 34.28	4.164 69.47	4.100 65.54	3.743 72.26	3.901 70.72	3.696, 3.902 64.17		
α-Kdop-(2→	D	ND	100.31	1.768, 2.149 35.16	4.090 66.89	4.050 67.06	3.600 73.54	3.989 70.68	3.760, 4.021 64.29		
<b><i>Bm_wadC<sub>per</sub></i> OS2</b>											
→6)-α-D-GlcpN3N1P	A	5.448 93.95	3.038 54.18	3.249 55.02	3.572 68.66	4.143 72.43	3.751, 4.267 70.15				
→6)-β-D-GlcpN3N4P-(1→	B	4.600 103.82	2.811 55.32	3.219 58.54	3.818 70.69	3.744 76.41	3.489, 3.809 63.34				
→4)-α-Kdop-(2→	C	ND	100.50	1.948, 1.993 34.24	4.175 69.49	4.101 65.45	3.741 72.22	3.901 70.58	3.695, 3.900 64.04		
→4)-α-Kdop-(2→	D	ND	100.36	1.848, 2.290 33.05	4.241 75.71	4.277 66.59	3.635 73.30	3.987 70.49	3.757, 4.018 64.16		
β-D-Glcp-(1→	E	4.636 102.31	3.292 73.83	3.515 76.44	3.408 70.35	3.485 76.63	3.746, 3.921 61.40				C4, D

<sup>a</sup> δ<sub>H4</sub> of residue C\* ~4.156.

glycerol 3-phosphate, 3.858/72.19, 3.822/65.52, 3.787/65.52, 3.686/63.11, and 3.616/63.11 ppm) were in agreement with data previously reported in the literature (39, 40). Diffusion-filtered experiments (<sup>1</sup>H NMR and <sup>1</sup>H,<sup>1</sup>H TOCSY spectra) were employed to confirm that these compounds had lower masses than the deacylated LOS material of *Bm\_manB<sub>core</sub>* and thus were not linked to LPS. The genome of *B. melitensis* contains an LptA homologue putatively involved in the transference of ethanolamine to an unknown position of the core-lipid A, which could account for the 2-aminoethyl phosphate group (16). This may have been substituting the O4 position of residue **B** (either as phosphodiester or diphosphodiester), but under the basic conditions used to prepare the oligosaccharides, this was probably lost (41–43). Additional spin systems of lower intensity, similar to **A** and **B** but with slightly different chemical shifts, were also identified in the <sup>1</sup>H,<sup>1</sup>H TOCSY spectra (**A'**: 5.406, 2.848, 3.106, 3.480, and 4.093, and **B'**: 4.516, 2.762, 3.152, 3.830, and 3.737, from H1 to H5, respectively), as well as resonances in the <sup>1</sup>H NMR at 1.286 (CH<sub>2</sub>) and 0.869 (CH<sub>3</sub>) ppm, attributed to residual acyl groups. The structure of the penta- and tetrasaccharide components of the LOS from *Bm\_manB<sub>core</sub>* are shown in Fig. 4A and are consistent with the structure of the lipid A reported previously for *B. abortus* (44).

**LOS from *BmEPR***—The <sup>1</sup>H NMR spectrum of the deacylated LOS (Fig. 5A, top) revealed a complex material, with several signals of different intensities in the anomeric region (between 5.42 and 4.43 ppm). Eight distinctive spin systems originating from the anomeric protons were identified in the <sup>1</sup>H,<sup>1</sup>H

TOCSY spectra, and the different sugar residues were denoted **A, F, G, E, B, J, H,** and **I**, in order of decreasing <sup>1</sup>H chemical shifts. In addition, a minor spin system similar to residue **F** but with slightly different chemical shifts was also identified and denoted **F\***. For residues **A, G, E, B, J, H,** and **I**, all protons from H1 to H6 could be identified in the <sup>1</sup>H,<sup>1</sup>H TOCSY spectrum recorded with the longest mixing time (Fig. 5B), indicating that these monosaccharide components have the *gluco*-configuration. The distinctive downfield chemical shift of H2 in residues **F** and **F\*** suggested that these are Man residues. The anomeric proton of residue **A** is a doublet of doublets (<sup>3</sup>J<sub>H1,H2</sub> = 3.2 Hz and <sup>3</sup>J<sub>P,H1</sub> = 8.3 Hz) indicating that this could be the α-D-GlcpN3N1P residue at the reducing end of the lipid A moiety. <sup>13</sup>C chemical shifts were assigned using multiplicity-edited <sup>1</sup>H,<sup>13</sup>C HSQC (Fig. 5C, left), <sup>1</sup>H,<sup>13</sup>C-H2BC, <sup>1</sup>H,<sup>13</sup>C HMBC, and <sup>1</sup>H,<sup>13</sup>C HSQC TOCSY experiments. <sup>1</sup>H and <sup>13</sup>C chemical shifts assignments are compiled in Table 4. Both C2 and C3 resonances of residues **A** and **B** were found in the region between 54 and 59 ppm, confirming that these are the two GlcN3N residues of the lipid A. The C2 resonances of residues **G, J, H,** and **I** were also found in the region of the nitrogen-bearing carbons, indicating that these are GlcN residues (Fig. 5C, left top); thus, residue **E** is Glc. <sup>1</sup>J<sub>C1,H1</sub> couplings constants were extracted from a coupled <sup>1</sup>H,<sup>13</sup>C HSQC spectrum and revealed that residues **A** and **F** are α-linked (<sup>1</sup>J<sub>C1,H1</sub> = 173–174 Hz), whereas residues **B, E** and **G–J** are β-linked (<sup>1</sup>J<sub>C1,H1</sub> = 162–165 Hz). The spin systems of the Kdo residues were analyzed as described before, and four distinctive populations were found and denoted **D** and **C**

## Brucella melitensis Rough LPS

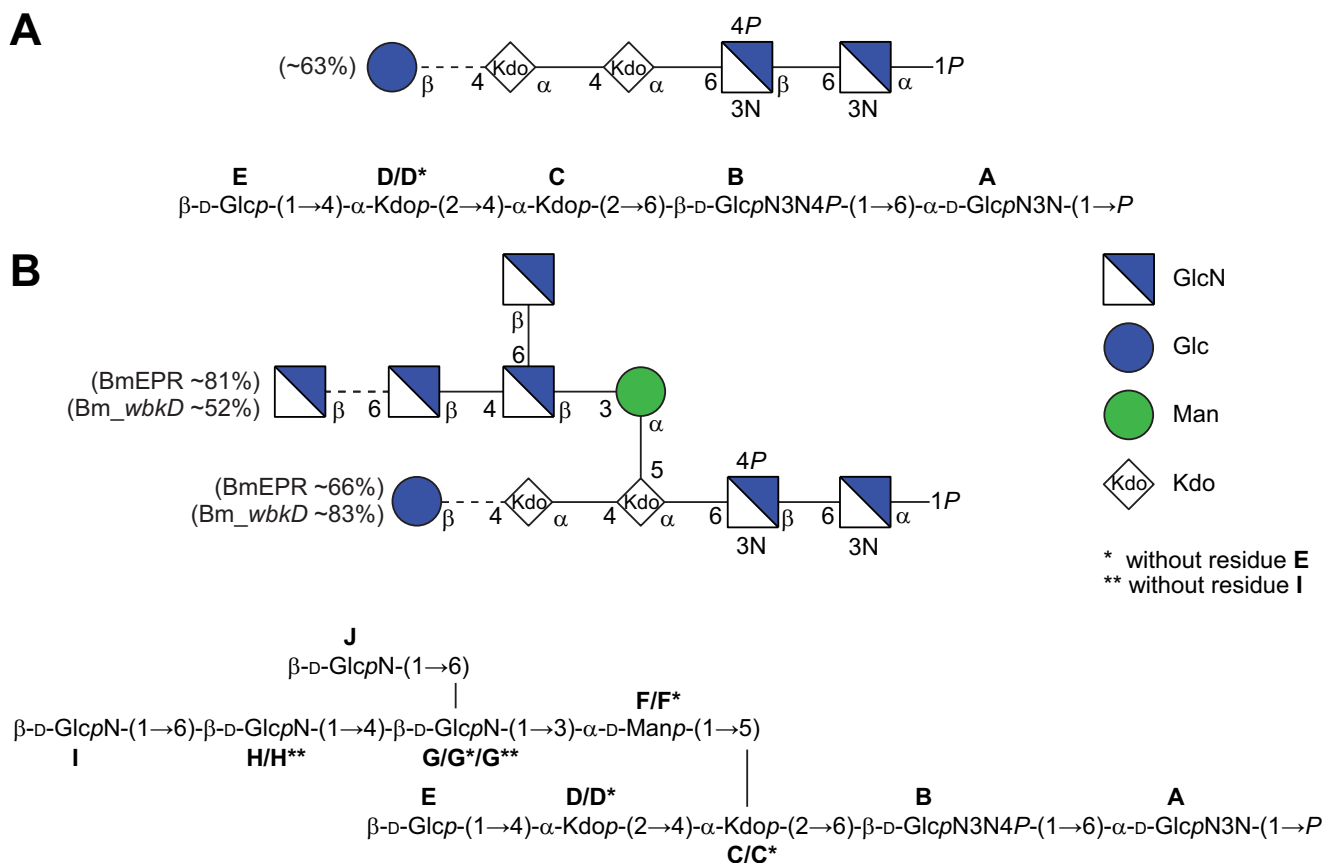


**FIGURE 4. Structures of the deacylated LOS from Bm\_manB<sub>coreI</sub>, Bm\_wbkD, and BmEPR.** A, structure of the penta- and tetra-saccharides in CFG format (top) and standard nomenclature (bottom) obtained by deacylation of the LOS from Bm\_manB<sub>coreI</sub>. B, structure of the deca-, nona-, and octasaccharides in CFG format (top) and standard nomenclature (bottom) obtained by deacylation of the LOS from BmEPR and Bm\_wbkD. The ratio of the different oligosaccharides present in the samples was estimated by integration of selected cross-peaks in the multiplicity-edited <sup>1</sup>H,<sup>13</sup>C HSQC spectrum; the **D3b** and **D3b\*** resonances were used to estimate the ratio of oligosaccharides with and without residue **E**, whereas the **G4** and **G4\*\*** resonances were used to estimate the ratio of oligosaccharides with and without residue **I**.

(major populations) and **D\*** and **C\*** (minor populations). Inter-residue correlations from anomeric carbons and protons were extracted from both regular and band-selective <sup>1</sup>H,<sup>13</sup>C HMBC spectra and used for determination of the sequence of sugar residues in the LOS (Table 4). The same two basic structures as for the LOS from Bm\_manB<sub>coreI</sub> could be identified (i.e. **E-D-C-B-A** and **D\*-C-B-A**), with the only difference being a branched oligosaccharide moiety composed of GlcN residues (**I-H-[J]G**), in the case of the major component that extends from a Man residue (**F**) linked to position 5 of the Kdo residue **C**. Thus, the major deca-saccharide and nonasaccharide components of the LOS (~66 and ~34%, respectively, determined by integration of the characteristic C3/H3b cross-peaks of residues **D** and **D\*** in the <sup>1</sup>H,<sup>13</sup>C HSQC spectrum) have the following sequence of sugar residues: **E-D-[I-H-[J]G-F]C-B-A** and **D\*-[I-H-[J]G\*-F\*]C\*-B-A**. The substitution positions of the phosphomonoester groups were studied as described above. The two major resonances in the <sup>31</sup>P NMR spectrum (2.5 and 3.1 ppm) were attributed to  $\alpha$ -D-GlcpN3N1P (residue **A**) and  $\alpha$ -D-GlcpN3N4P (residue **B**); likewise, the minor resonances found at  $\delta_p$  4.0, 4.1, and 4.4 were attributed to free ethanolamine phosphate, glycerol 2-phosphate, and glycerol 3-phosphate. Additional cross-peaks of lower intensity (~19%) were also found in the multiplicity edited <sup>1</sup>H,<sup>13</sup>C HSQC spectrum and attributed to an

oligosaccharide similar to the deca-saccharide described above, but without the GlcN residue **I** linked to residue **H**. In this case, <sup>1</sup>H and <sup>13</sup>C chemical shift assignments were carried out by comparison with the chemical shifts of the same oligosaccharide found in the LOS from Bm\_wbkD (~48%) (see below), and the corresponding sugar residues were denoted with a double asterisk. The C4/H4 cross-peaks of residues **G** and **G\*\*** in the <sup>1</sup>H,<sup>13</sup>C HSQC spectrum were used to estimate the percentage of these oligosaccharides in the sample. The structures of the deca- and nonasaccharide components of the LOS from BmEPR are shown in Fig. 4B.

**LOS from Bm\_wbkD**—The <sup>1</sup>H NMR spectrum of the deacylated LOS from Bm\_wbkD (Fig. 5A, bottom) appears quite similar to that of BmEPR (Fig. 5A, top), with the only difference being the relative intensities displayed by some of the resonances. <sup>1</sup>H and <sup>13</sup>C chemical shifts assignments were carried out as described previously; the same oligosaccharide structures as above were identified, **E-D-[I-H-[J]G-F]C-B-A** and **D\*-[I-H-[J]G\*-F\*]C\*-B-A**, and particularly the nonasaccharide **E-D-[H\*\*-[J]G\*\*]-F\*\*]C\*-B-A**, that was fully characterized due to the higher relative concentration of the component in the sample (~48%, instead of 19% observed in the case of BmEPR). Comparison of the multiplicity-edited <sup>1</sup>H,<sup>13</sup>C HSQC spectrum of the deacylated LOS from BmEPR (Fig. 5C, bottom left) and

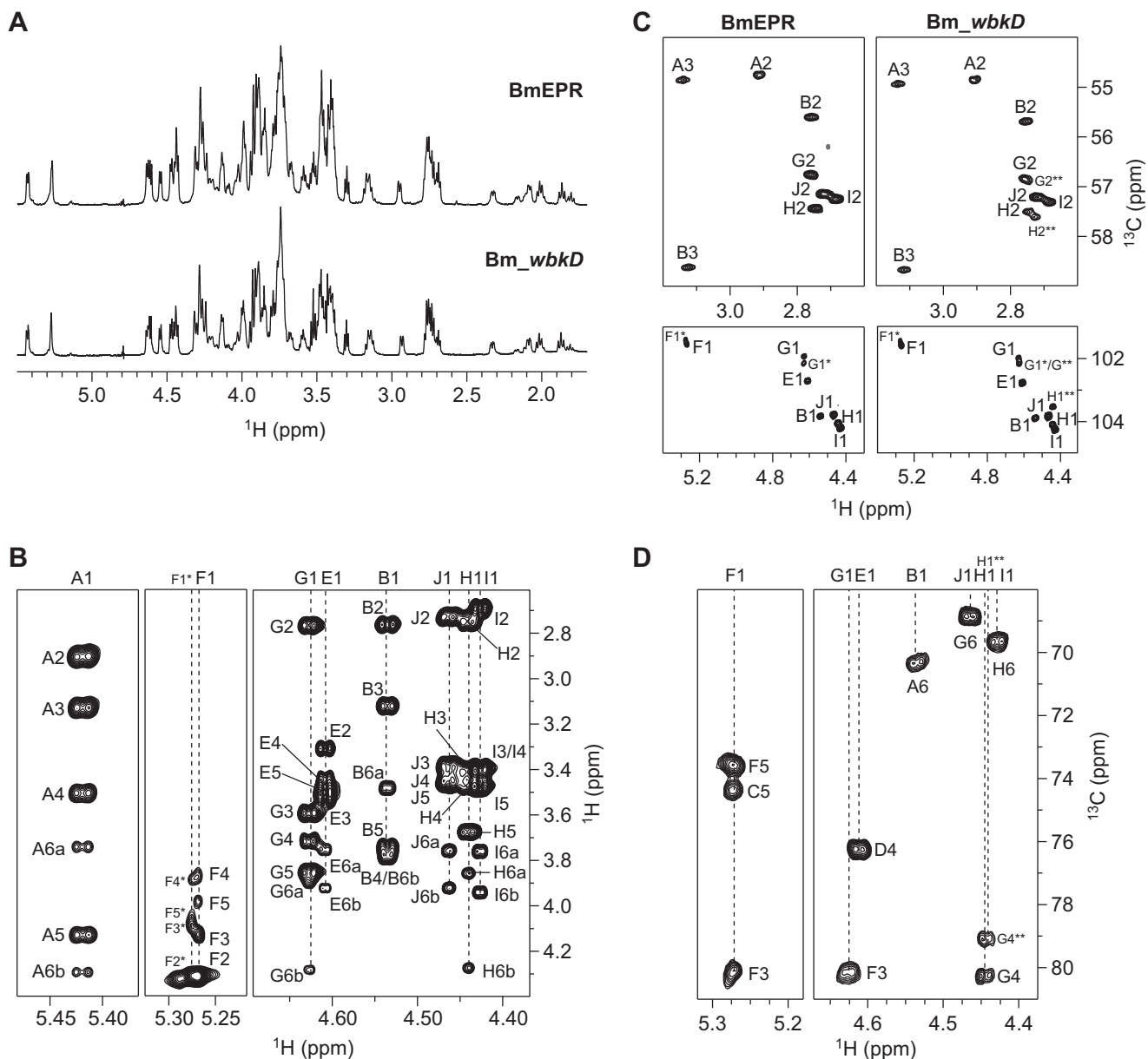


FIGURE 5. NMR spectra of the deacylated LOS from *Bm\_wbkD* and *BmEPR*. A, comparison of the diffusion-filtered  $^1\text{H}$  NMR spectra of the deacylated LOS from *BmEPR* and *Bm\_wbkD* (top and bottom, respectively). B, selected regions of the  $^1\text{H},^1\text{H}$  TOCSY ( $\tau_m = 100$  ms) of deacylated LOS from *BmEPR* showing correlations from anomeric protons. C, comparison of selected regions of the multiplicity-edited  $^1\text{H},^{13}\text{C}$  HSQC spectrum of the deacylated LOS from *BmEPR* and *Bm\_wbkD* (left and right, respectively), showing part of the anomeric region (bottom) and the region for the nitrogen-bearing carbons (top). D, selected regions of the  $^1\text{H},^{13}\text{C}$  HMBC spectrum of the deacylated LOS from *Bm\_wbkD* showing intra- and inter-residue correlations from anomeric protons.

that of *Bm\_wbkD* (Fig. 5C, bottom right) allowed for the identification of a conspicuous resonance at  $\delta_{\text{H}}/\delta_{\text{C}}$  4.440/103.48 (H1/C1 in residue **H\*\***) that is noticeably stronger in the latter spectrum. The  $^1\text{H}$  and  $^{13}\text{C}$  resonances of residue **H\*\*** were assigned employing  $^1\text{H},^1\text{H}$  TOCSY,  $^1\text{H},^{13}\text{C}$  HSQC TOCSY, and  $^1\text{H},^{13}\text{C}$  HMBC experiments. The H6a and H6b resonances (3.752 and 3.934 ppm, respectively) were identified in the  $^1\text{H},^1\text{H}$  TOCSY spectrum ( $\tau_m = 100$  ms) due to their significant chemical shifts differences with respect to those of H6a and H6b in residue **H** and were correlated to the C6 carbon in the multiplicity-edited  $^1\text{H},^{13}\text{C}$  HSQC spectrum. The differences in the chemical shifts of C6 in residues **H\*\*** and **H** (61.46 and 69.66 ppm, respectively) indicated that the former is not 6-substituted and thus is a terminal residue. Another conspicuous signal was observed in

the multiplicity-edited  $^1\text{H},^{13}\text{C}$  HSQC spectrum at  $\delta_{\text{H}}/\delta_{\text{C}}$  3.736/79.12 (H4/C4 in residue **G\*\***); the  $^1\text{H}$  resonances in that spin system were identified using correlations from the carbon at 79.12 ppm in the  $^1\text{H},^{13}\text{C}$  HSQC TOCSY spectrum ( $\tau_m = 100$  ms), and the corresponding  $^{13}\text{C}$  resonances were assigned using a multiplicity-edited  $^1\text{H},^{13}\text{C}$  HSQC spectrum. Furthermore, an inter-residue correlation was observed in the band-selective constant-time  $^1\text{H},^{13}\text{C}$  HMBC spectrum (recorded with enhanced resolution in the carbon anomeric region) between the anomeric carbon of residue **H\*\*** and the proton at 3.736 ppm (H4 in residue **G\*\***). In addition, the regular  $^1\text{H},^{13}\text{C}$  HMBC spectrum showed a correlation between the anomeric proton of residue **H\*\*** and the C4 carbon in residue **G\*\*** (Fig. 5D), thus confirming that the **G\*\*** residue is 4-substituted with residue

**TABLE 4**

**NMR chemical shifts assignments of the resonances of the LOS from BmEPR and Bm\_wbkD**

<sup>1</sup>H, <sup>13</sup>C, and <sup>31</sup>P NMR chemical shifts (ppm) at 25 °C and pD 8 of the resonances of the components of the deacylated LOS from BmEPR and Bm\_wbkD and inter-residue correlations from the <sup>1</sup>H, <sup>13</sup>C HMBC spectra. The different oligosaccharide components of the samples differ in the presence/absence of residues E (Glc) and/or I (GlcN) (see Fig. 4). For residue A, <sup>3</sup>J<sub>P,H1</sub> = 8.3 Hz, <sup>2</sup>J<sub>P,C1</sub> = ~4.5 Hz, and <sup>3</sup>J<sub>P,C2</sub> = ~7.4 Hz. Resonances from H1 and C1 in residue G\* are found at 4.626 and 102.12 ppm, respectively (overlapping with H1 and C1 in residue G\*\*). Resonances from H3 and C3 in F\*\* are found at 4.129 and 80.07 ppm (overlapping with H3 and C3 in residue F). ND means not determined. NR means not resolved.

Sugar residues		<sup>1</sup> H/ <sup>13</sup> C										<sup>31</sup> P	HMBC correlations (from anomeric atom)			
		1	2	3a	3b	4	5	6a	6b	7	8a			8b		
→6)-α-D-GlcpN3N1P	A	5.419 (3.2)	2.898	3.126		3.503	4.127	3.738	4.290						2.5	
→6)-β-D-GlcpN3N4P-(1→	B	4.535 (8.0)	2.753	3.112		3.764	3.724	3.472	3.782						3.1	C6, A H6a, A
→4,5)-α-Kdop-(2→	C			2.010	2.081	4.250	4.236	3.721 <sup>a</sup>			3.738 <sup>a</sup>	3.717	3.890			H6a, B
→4)-α-Kdop-(2→ (without residue E)	C*	175.68 <sup>a</sup>	100.45	35.25		70.54	74.36	72.80 <sup>a</sup>			70.46 <sup>a</sup>	64.27				
→4)-α-Kdop-(2→	D	ND	100.45	35.25	1.863	4.205	4.276	3.721			ND	ND	ND			
α-Kdop-(2→ (without residue E)	D*	175.34 <sup>a</sup>	101.18	33.25	2.324	76.22	66.68	72.83			3.987	3.793	3.996			H4, C
β-D-Glcp-(1→	E	ND	101.74	35.29	2.161	4.042	4.022	3.702			3.994	3.782	3.983			
→3)-α-D-Manp-(1→	F	4.609 (7.9)	3.299	3.520		66.77	67.37	72.96			71.03	64.85				C4, D H4, D
→3)-α-D-Manp-(1→ (without residue E)	F*	102.69 {162}	73.86	76.30		70.30	76.53	61.36								C5, C H5, C
→4,6)-β-D-GlcpN-(1→	G	5.268 (NR)	4.312	4.129		3.847	4.130	~3.887								
→4,6)-β-D-GlcpN-(1→ (without residue I)	G**	101.54 {173}	68.71	80.07		65.79	73.62	61.66								H5, C*
→6)-β-D-GlcpN-(1→	H	5.275	4.310	4.089		3.874	4.089	~3.887								C3, F H3, F
β-D-GlcpN-(1→ (without residue I)	H**	101.40 {173}	68.90	80.47		65.66	73.41	61.66								H3, F**
β-D-GlcpN-(1→	I	4.627 (8.2)	2.758	3.584		3.709	3.844	3.891	4.272							C4, G H4, G
β-D-GlcpN-(1→	J	101.91 {165}	56.77	75.20		80.26	74.25	68.89								C4, G** H4, G**
β-D-GlcpN-(1→	J	4.626 (8.30)	2.756	3.595		3.736	3.844	3.891	4.272							C6, H H6a, H C6, G
		102.12 {165}	56.87	74.90		79.12	74.25	68.89								
		4.442 (8.1)	2.748	3.405		3.467	3.668	3.851	4.267							
		104.03 {163}	57.45	76.01		70.48	75.70	69.66								
		4.440	2.727	3.405		3.480	3.489	3.752	3.934							
		103.48 {163}	57.59	76.31		70.41	77.03	61.46								
		4.426 (8.1)	2.682	3.384		3.464	3.460	3.752	3.934							
		104.18 {163}	57.26	76.33 <sup>b</sup>		70.55	76.87	61.62								
		4.465 (8.2)	2.723	3.373		3.409	3.460	3.748	3.913							
		103.77 {162}	57.16	76.30 <sup>b</sup>		70.55	76.87	61.57								

<sup>a</sup> Tentative assignments are shown.

<sup>b</sup> Assignments may be interchanged.

**H\*\*.** Furthermore, the anomeric carbon of residue G\*\* showed an inter-residue correlation in the band-selective constant-time <sup>1</sup>H, <sup>13</sup>C HMBC spectrum to a proton at 4.129 ppm, attributed to H3 of residue F\*\* (overlapping with H3 of residue F). <sup>1</sup>H and <sup>13</sup>C chemical shifts assignments of the deca- and nonasaccharide components of the LOS from Bm\_wbkD are compiled in Table 4; the corresponding structures and relative percentages are shown in Fig. 4B.

**LOS from Bm\_wadC\_per**—Two oligosaccharides were isolated from the deacylated LOS of the double mutant, viz. a tetra- and a pentasaccharide (OS1 and OS2, respectively), the structures of which correspond to those described for the oligosaccharide mixture from Bm\_manB\_core. Their <sup>1</sup>H and <sup>13</sup>C NMR chemical shifts (Table 3) were assigned by two-dimensional NMR experiments (cf. <sup>1</sup>H, <sup>13</sup>C HSQC NMR spectra in Fig. 6, A and B, respectively), in good agreement with those from the Bm\_manB\_core oligosaccharides. In particular, an interglycosidic heteronuclear correlation was present in the <sup>1</sup>H, <sup>13</sup>C HMBC spectrum of the pentasaccharide from the anomeric proton (H1) of the glucosyl residue to the glycosyloxylated carbon atom (C4) of the second Kdo residue (Fig. 6C), thus establishing and confirming the structural element E-D (Fig. 4).

In a recent investigation of oligo- and polysaccharides obtained by mild acid hydrolysis of LPS from different *Brucella* serotypes, structural elements consistent with core oligosaccharides presented herein were present (15). Notably, it was shown that D-QuiNAc, which is the primer for the O-chain polysaccharide, is β-(1→4)-linked to the glucose residue of the core (B.

*suis* data), thereby defining the attachment site of the O-antigen to the core region of *Brucella* serotypes, a finding anticipated to be valid in the *Brucella* serotypes investigated herein.

**Role of *Brucella Melitensis* Core in Virulence**

For an unambiguous analysis of the role of the LPS core in the virulence of *B. melitensis*, the use of core-defective O-PS-bearing bacteria is necessary. To this end, a mutant in *wadC* was constructed. As shown in Fig. 7, SDS-PAGE and Western blot analyses show that this *wadC* mutant carries a core defect but keeps the O-PS, a result in agreement with previous work in *B. abortus* (17). This phenotype is consistent with the putative role of WadC as a mannosyltransferase because this enzymatic activity would be necessary to create the mannose-Kdo linkage in the structure shown in Fig. 4B. To verify this, a double Bm\_wadC\_per mutant was constructed and its LOS analyzed. Consistent with the role of Per in O-PS synthesis (Fig. 1) and the need of the O-PS for export to the periplasm and subsequent linkage to the core oligosaccharide (5), the LOS of this double mutant lacked the full O-PS section (quinovosamine, mannose, and *N*-formyl perosamine polymer). Moreover, this LOS also completely lacked the mannose/glucosamine-containing oligosaccharide linked to Kdo (residue C), being similar to that of the *manB\_core* mutant (blocked in mannose synthesis). The lack of aminosugars should increase the negative charge of the inner sections of LPS, and this was shown to occur in ζ<sub>sm</sub> potential measurements of the Bm\_wadC\_per mutants and Bm\_per (Fig. 8).

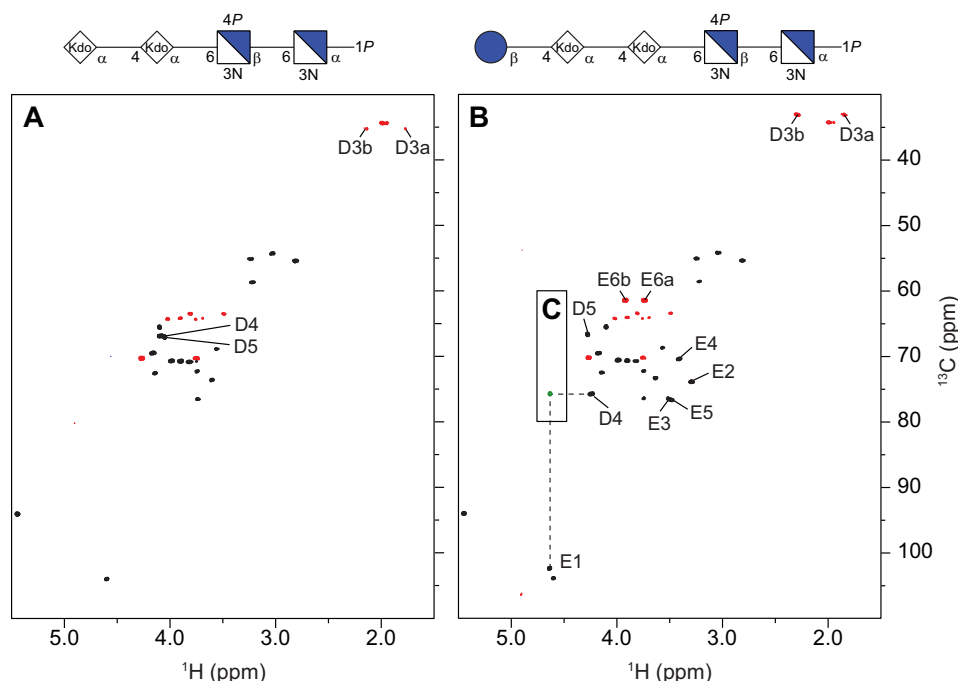


FIGURE 6. **NMR spectra of the deacylated LOS from *Bm\_wadC\_per*.** Comparison of the multiplicity-edited  $^1\text{H}$ ,  $^{13}\text{C}$  HSQC spectra (black/red) of the tetrasaccharide (A) and pentasaccharide (B) (OS1 and OS2, respectively) isolated from *Bm\_wadC\_per*; the cross-peaks with significant chemical shift differences between the two oligosaccharides are annotated. The structures (in CFG format) of the respective oligosaccharides are shown on the top of each spectra. C, overlay of a selected region of the  $^1\text{H}$ ,  $^{13}\text{C}$  HMBC spectrum of the OS2 showing an interglycosidic heteronuclear long range correlation (green) between residues D and E.

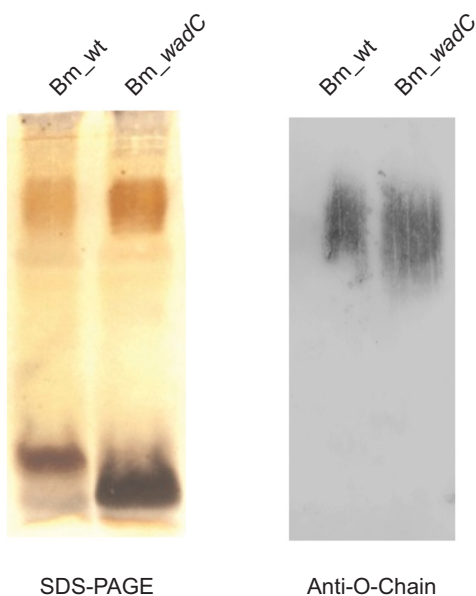


FIGURE 7. ***B. melitensis* WadC mutants carry a core defect that does not affect the linkage to the O-PS.** SDS-PAGE and Western blot analysis with anti-O-chain monoclonal antibody Cby-33H8 of LPS SDS-proteinase K extracts from *Bm\_wt* (*B. melitensis* 16M wild type) and *Bm\_wadC* (*B. melitensis* 16M $\Delta$ wadC mutant).

To assess the biological effect of the core, the ability of *Bm\_wadC* to multiply in BMDCs was studied in comparison with wild type *B. melitensis*. Mutant bacteria displayed a comparatively reduced ability to multiply in these cells suggestive of attenuation (Fig. 9A). When the virulence was assessed *in vivo* using the mouse model of brucellosis, *Bm\_wadC* and the parental strain yielded similar cfu at post-infection week 2 (Fig. 9B).

At post-infection week 8, however, the mutant was present in comparatively reduced numbers in the spleens (Fig. 9C).

To determine whether the reduced virulence of *Bm\_wadC* was associated with an alteration in the immunogenicity of its LOS structure, further experiments were performed to assess its potential to induce pro-inflammatory responses in BMDCs. Unlike the *Bm\_wt* LPS, which induced no secretion of inflammatory cytokines, *Bm\_wadC* LPS induced the release of the pro-inflammatory cytokines IFN- $\gamma$ , IL-12p40, IL-6, and TNF- $\alpha$  at high levels that were comparable with those obtained with LPS from *E. coli* (Fig. 10A). Similarly, with *E. coli* LPS, *Bm\_wadC*-stimulated BMDCs underwent maturation as judged by the surface expression of MHC-II and the co-stimulatory markers CD86, CD80, and CD40. By contrast, BMDCs treated with *Bm\_wt* LPS maintained an immature phenotype with no evident up-regulation of these surface receptors (Fig. 10B). Taken together, these results demonstrate that an intact LPS core is not only required for full virulence of *B. melitensis*, but it also contributes to limiting the activation and maturation of dendritic cells while undergoing replication in these target cells. An alteration in the LPS core, as demonstrated here with *Bm\_wadC*, would appear to confer a more endotoxigenic phenotype rendering the pathogen more visible to host target cells, attenuating its intracellular replicative capacity and virulence in mice.

### Discussion

Rough mutants of *B. melitensis* have been reported to show attenuated responses with respect to strains having a smooth LPS. In addition, phenotypes with different core defect structures have been observed to give rise to different attenuation

## Brucella melitensis Rough LPS

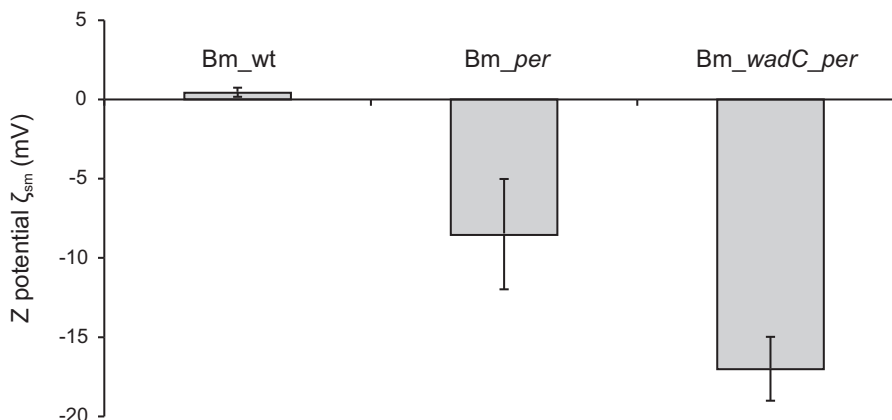


FIGURE 8. *B. melitensis* core lateral branch shields bacterial surface negatively charged groups (inner core and lipid A). The figure presents  $\zeta$  potential measurements of Bm\_per (no LPS O-PS and complete core oligosaccharide), Bm\_wadC\_per (no LPS O-PS and defective core oligosaccharide) in comparison with *B. melitensis* 16M (wild type strain; Bm\_wt). Each bar represents the means  $\pm$  S.E. of 10 measurements of one representative experiment.

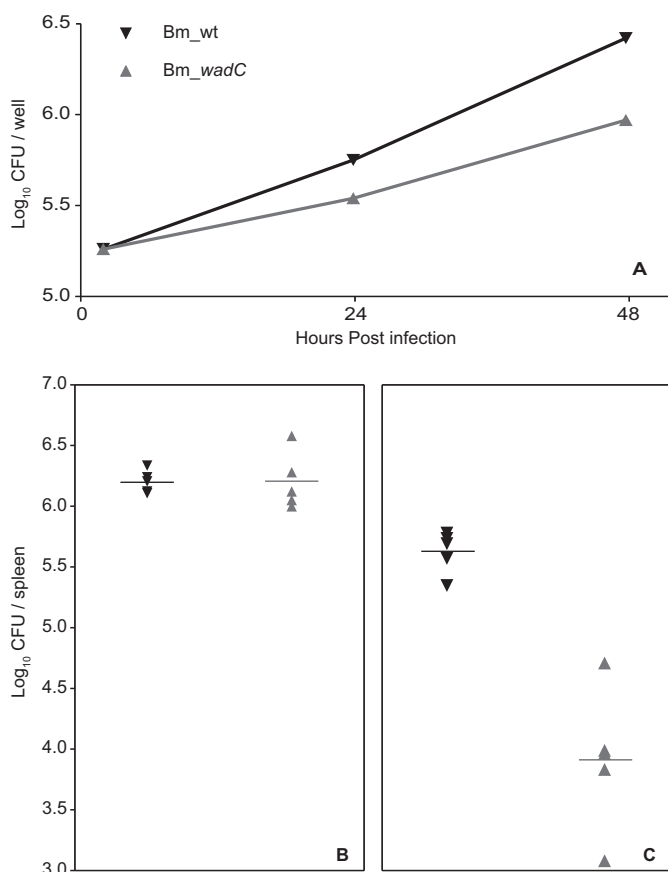


FIGURE 9. *B. melitensis* mutants defective in the core lateral branch are attenuated in dendritic cells and in mice. Bone marrow-derived dendritic cells were infected with *B. melitensis* 16M (wild type strain; Bm\_wt) or *B. melitensis* 16M $\Delta$ wadC (Bm\_wadC), and CFU were measured at the indicated times (each point represents the means  $\pm$  S.E. of triplicate wells of a representative experiment) (A). Groups of five mice were infected with  $5 \times 10^4$  CFU of Bm\_wt (▼) or Bm\_wadC (▲) and CFU/spleen determined at 2 (B) and 8 (C) weeks.

patterns, and this has been associated with changes on the bacterial surface (10, 17). Therefore, knowledge of the primary structure of the LOS may help not only to have a better understanding of the genetics involved in biosynthetic processes but also to comprehend the interaction of the bacteria with the host

immune system. Herein, we present a comprehensive study of the structures of different LOSs extracted from four *B. melitensis* strains. These include the native R-LPS (LOS) obtained from a strain producing increased proportions of R-LPS (18) (BmEPR), a mutant in which the *wbkD* gene was disrupted (Bm\_wbkD) and a mutant affected in the ManB<sub>core</sub> protein (Bm\_manB<sub>core</sub>) as well as the double mutant strain Bm\_wadC\_per.

The structural elucidation of the deacylated LOSs from BmEPR and Bm\_wbkD, carried out using NMR spectroscopy, revealed that both mutants are capable of producing a complete core structure (Fig. 4B) as well as minor components lacking the terminal residue I (19 and 48%, respectively) and/or residue E (34 and 17%, respectively). Furthermore, the pseudo-molecular ions observed in the mass spectra of the deacylated LOS from Bm\_wbkD (Fig. 2B and Table 2) were in agreement with the two major components determined by NMR spectroscopy as follows: (i) a complete core deca-saccharide with a molecular formula of C<sub>64</sub>H<sub>116</sub>N<sub>8</sub>O<sub>53</sub>P<sub>2</sub> that is consistent with a structure containing two Hex (Glc and Man), four HexN (GlcN), two Kdo, and two HexNN residues bearing phosphomonoester substituents (GlcN3N1P and GlcN3N4P), and (ii) a nonasaccharide with a molecular formula of C<sub>58</sub>H<sub>104</sub>N<sub>7</sub>O<sub>49</sub>P<sub>2</sub> that is consistent with the same components as above but having three GlcN residues instead of four. It needs to be stressed that the full structures obtained for BmEPR and Bm\_wbkD are identical. *B. melitensis* EP was used in this work because it keeps the ability to synthesize S-LPS while producing increased amounts of R-LPS, which makes possible to obtain larger amounts of a native R-LPS for chemical analysis. Because a complete core structure was present in the LOS from Bm\_wbkD, the *wbkD* gene can be anticipated to encode for a protein involved in the biosynthesis of the O-PS. This is in agreement with the predicted function of WbkD as involved in the biosynthesis of QuiNAc, the undecaprenol-priming residue and therefore the first sugar of the O-PS chain (Fig. 1) (10). In a smooth LPS the O-PS chain, having a 3-substituted QuiNAc residue located at its reducing end, would be extended from the O4 position of the Glc residue (15). Consequently, the pentasaccharide moiety

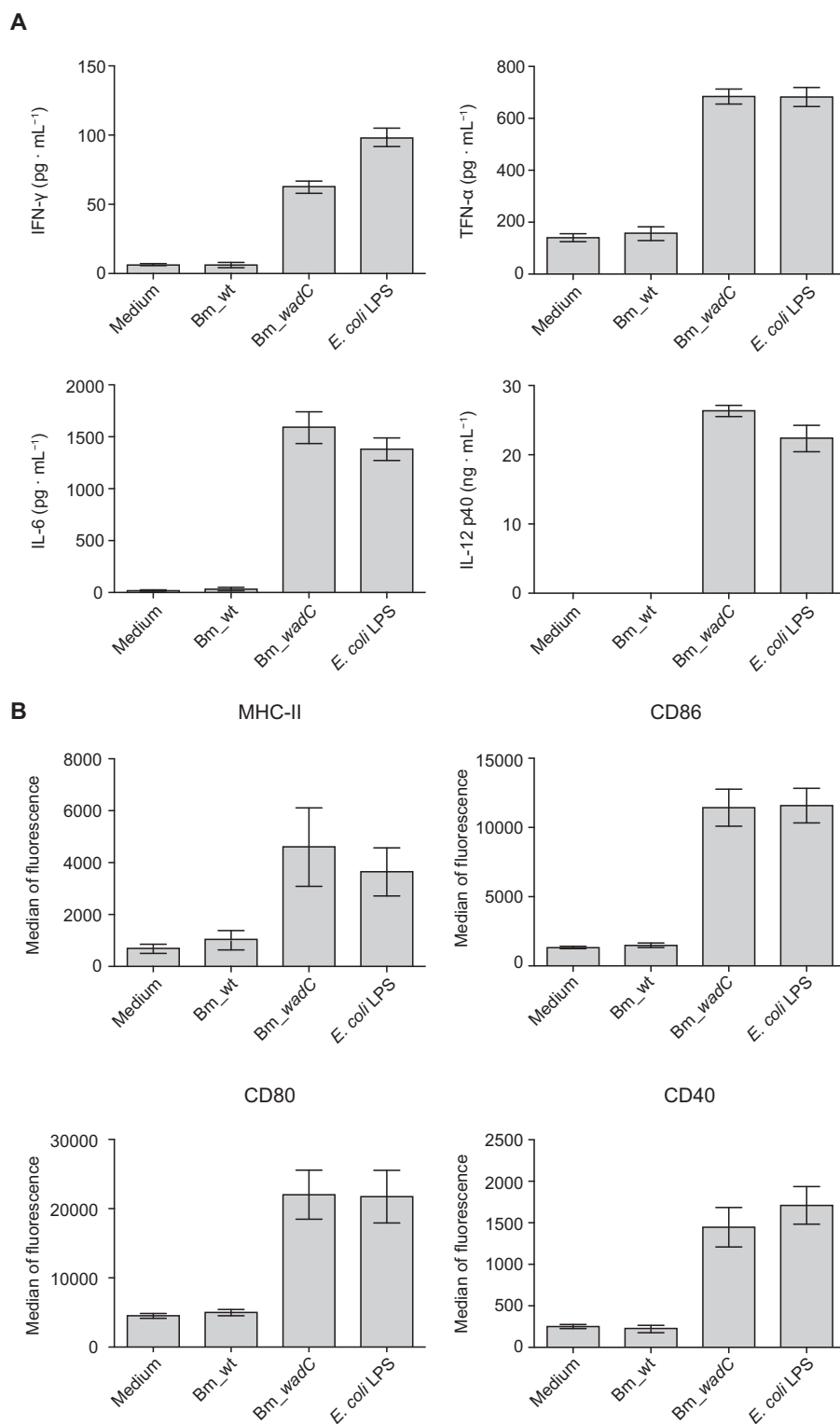


FIGURE 10. *B. melitensis wadC* LPS triggers dendritic cell activation and maturation. Mouse BMDCs were stimulated for 24 h with medium or purified LPS from *B. melitensis* 16M (wild type strain; Bm\_wt), *B. melitensis* 16MΔwadC (Bm\_wadC), or *E. coli* (O55:B5), all administered at an equivalent molarity (0.25 μM). IFN-γ, TNF-α, IL-6, and IL-12p40 secretion levels in culture supernatant were determined by ELISA (A). Surface levels of MHC-II, CD86, CD80, and CD40 were measured by flow cytometry (B). Data are presented as the means ± S.E. of at least five independent experiments.

composed of GlcN residues linked to a mannosyl residue constitutes a core branch.

The mutant in the *manB<sub>core</sub>* gene showed a deeply truncated core (Fig. 4A) in which the lateral branch is absent. This is in agreement with previous observations that such a kind of

mutants (Bm\_*manB<sub>core</sub>*) have a lower molecular mass LOS (R3 phenotype) than those of BmEPR and Bm\_wbkD (R1 phenotype) and fail to react with monoclonal antibodies specific for the outer core (10, 16). The studies carried out using NMR spectroscopy showed that the LOS from Bm\_*manB<sub>core</sub>* is com-

posed of two major oligosaccharide components as follows: a pentasaccharide and a tetrasaccharide (63 and 37%, respectively), with the only difference being the presence or absence of the terminal Glc residue, respectively (Fig. 4A). These structures are in agreement with the two sets of pseudo-molecular ions observed in the mass spectrum that correspond to structures of general formula  $C_{34}H_{62}N_4O_{32}P_2$  and  $C_{28}H_{52}N_4O_{27}P_2$  (Fig. 2A and Table 2), respectively. The ManB<sub>core</sub> has been previously predicted to be the phosphomutase involved in the biosynthesis of GDP-mannose (Fig. 1), which is used in the biosynthesis of monosaccharide components of the core and O-PS. Indeed, it is shown here that when the *manB<sub>core</sub>* gene is blocked the LOS oligosaccharide lacks the mannosyl residue and the branched structure that extends from it.

From a biological point of view, the structure described here is not a trivial one as it explains a number of characteristics related to the virulence of an important pathogen. The brucellae are resistant to components of the innate immune system such as bactericidal peptides and complement while prompting a weak pro-inflammatory response during infection (7), characteristics that are in part related to the biological and physicochemical properties of its LPS (6, 7, 17). Many of these properties have been attributed to the poor cytokine-inducing characteristics of *Brucella* lipid A, on account of its very long chain fatty acids that may prevent effective recognition by TLR4-MD2 (6). However, it has been predicted that the core should play a complementary role whereby its structure allows it to conceal the inner sections of lipid A, making them less accessible for binding by the TLR4-MD2 complex or for binding bactericidal peptides or complement (15, 17). The loss in monoclonal antibody reactivity observed with a *B. abortus wadC* mutant suggested that the core of smooth brucellae may atypically be composed of two separate oligosaccharide branches, one linking the lipid A to the O-PS and another that protrudes laterally thereby concealing the negatively charged groups essential for interaction with the TLR4-MD2 complex (17). The characterization presented here confirms these predictions as the GlcN-rich oligosaccharide stemming from the first Kdo residue (C) also creates a positively charged structure that can neutralize the negatively charged groups of Kdo and lipid A, the primary targets of innate immunity receptors and effector molecules. This is further supported by the attenuated intracellular replicative/virulence profile and change in surface charge exhibited by the Bm\_ *wadC* mutant strain, as well as the enhanced ability of its LPS to stimulate maturation and pro-inflammatory cytokine secretion (including Th1-type cytokines IL-12 and IFN- $\gamma$ ) when compared with its WT counterpart.

In addition to reaffirming the above hypothesis, these observations provide new understanding of the important role of *Brucella* core-LPS in influencing key host-pathogen interactions during the early stages of infection and perhaps when chronic disease develops. Moreover, our findings have important implications as they identify *Brucella* LPS as a key target/protagonist for strategies aimed toward the development of safer attenuated brucellosis vaccines that can promote more efficient protective Th1 responses (45), thought to be critical for the control of intracellular brucellae.

**Author Contributions**—I. M. and G. W. conceived and coordinated the study. O. H., J. P. G., I. M., and G. W. supervised the study. C. F., R. C. A., J. S., M. I., Y. Z., V. A. G. and S. H. performed experiments and genomic analyses. C. F., R. C. A., J. S., I. M., and G. W. wrote the manuscript. All authors analyzed the results and approved the final version of the manuscript.

**Acknowledgments**—We thank Katharina Jakob, Hermann Moll, Heiko Kässner (all at Research Center Borstel), and Alberto Delgado for technical assistance and the Swedish NMR Centre at Gothenburg University for granting NMR spectrometer time. Advice by M. J. Grilló on the experiments in mice is also gratefully acknowledged.

## References

1. Dean, A. S., Crump, L., Greter, H., Schelling, E., and Zinsstag, J. (2012) Global burden of human brucellosis: a systematic review of disease frequency. *PLoS Negl. Trop. Dis.* **6**, e1865
2. McDermott, J., Grace, D., and Zinsstag, J. (2013) Economics of brucellosis impact and control in low-income countries. *Rev. Sci. Tech.* **32**, 249–261
3. Ariza, J. (1999) Brucellosis: an update. The perspective from the Mediterranean basin. *Rev. Med. Microbiol.* **10**, 125–135
4. Raetz, C. R., and Whitfield, C. (2002) Lipopolysaccharide endotoxins. *Annu. Rev. Biochem.* **71**, 635–700
5. Valvano, M. A., Furlong, S. E., and Patel, K. B. (2011) in *Bacterial Lipopolysaccharides* (Knirel, Y. A., and Valvano, M. A., eds) pp. 275–310, Springer-Verlag, Wien
6. Lapaque, N., Moriyon, I., Moreno, E., and Gorvel, J.-P. (2005) *Brucella* lipopolysaccharide acts as a virulence factor. *Curr. Opin. Microbiol.* **8**, 60–66
7. Barquero-Calvo, E., Chaves-Olarte, E., Weiss, D. S., Guzmán-Verri, C., Chacón-Díaz, C., Rucavado, A., Moriyón, I., and Moreno, E. (2007) *Brucella abortus* uses a stealthy strategy to avoid activation of the innate immune system during the onset of infection. *PLoS ONE* **2**, e631
8. Knirel, Y. A. (2011) in *Bacterial Lipopolysaccharides. Structure, Chemical Synthesis, Biogenesis and Interaction with Host Cells* (Knirel, Y. A., and Valvano, M. A., eds) pp. 41–115, Springer, Vienna
9. Zacccheus, M. V., Ali, T., Cloeckeaert, A., Zygmunt, M. S., Weintraub, A., Iriarte, M., Moriyón, I., and Widmalm, G. (2013) The epitopic and structural characterization of *Brucella suis* biovar 2 O-polysaccharide demonstrates the existence of a new M-negative C-negative smooth *Brucella* serovar. *PLoS ONE* **8**, e53941
10. González, D., Grilló, M.-J., De Miguel, M.-J., Ali, T., Arce-Gorvel, V., Delrue, R.-M., Conde-Alvarez, R., Muñoz, P., López-Goñi, I., Iriarte, M., Marín, C.-M., Weintraub, A., Widmalm, G., Zygmunt, M., Letesson, J.-J., et al. (2008) Brucellosis vaccines: assessment of *Brucella melitensis* lipopolysaccharide rough mutants defective in core and O-polysaccharide synthesis and export. *PLoS ONE* **3**, e2760
11. Turse, J. E., Pei, J., and Ficht, T. A. (2011) Lipopolysaccharide-deficient *Brucella* variants arise spontaneously during infection. *Front. Microbiol.* **2**, 54
12. Mancilla, M., López-Goñi, I., Moriyón, I., and Zárraga, A. M. (2010) Genomic island 2 is an unstable genetic element contributing to *Brucella* lipopolysaccharide spontaneous smooth-to-rough dissociation. *J. Bacteriol.* **192**, 6346–6351
13. Mancilla, M., Marín, C. M., Blasco, J. M., Zárraga, A. M., López-Goñi, I., and Moriyón, I. (2012) Spontaneous excision of the O-polysaccharide *wbkA* glycosyltransferase gene is a cause of dissociation of smooth to rough *Brucella* colonies. *J. Bacteriol.* **194**, 1860–1867
14. Zygmunt, M. S., Blasco, J. M., Letesson, J.-J., Cloeckeaert, A., and Moriyón, I. (2009) DNA polymorphism analysis of *Brucella* lipopolysaccharide genes reveals marked differences in O-polysaccharide biosynthetic genes between smooth and rough *Brucella* species and novel species-specific markers. *BMC Microbiol.* **9**, 92
15. Kubler-Kielbaso, J., and Vinogradov, E. (2013) The study of the core part and non-repeating elements of the O-antigen of *Brucella* lipopolysaccharide.

- Carbohydr. Res.* **366**, 33–37
16. Iriarte, M., González, D., Delrue, R. M., Monreal, D., Conde-Álvarez, R., López-Goñi, I., Letesson, J.-J., and Moriyón, I. (2004) in *Brucella: Molecular and Cellular Biology* (López-Goñi, I., and Moriyón, I., eds) pp. 159–192, Horizon Scientific Press Ltd., Norfolk, UK
  17. Conde-Álvarez, R., Arce-Gorvel, V., Iriarte, M., Manček-Keber, M., Barquero-Calvo, E., Palacios-Chaves, L., Chacón-Díaz, C., Chaves-Olarte, E., Martirosyan, A., von Bargen, K., Grilló, M.-J., Jerala, R., Brandenburg, K., Llobet, E., Bengoechea, J. A., *et al.* (2012) The lipopolysaccharide core of *Brucella abortus* acts as a shield against innate immunity recognition. *PLoS Pathog.* **8**, e1002675
  18. Bowden, R. A., Verger, J. M., Grayon, M., Limet, J. N., and Dubray, G. (1993) Simultaneous expression of smooth and rough phase properties related to lipopolysaccharide in a strain of *Brucella melitensis*. *J. Med. Microbiol.* **39**, 363–370
  19. Aragón, V., Díaz, R., Moreno, E., and Moriyón, I. (1996) Characterization of *Brucella abortus* and *Brucella melitensis* native haptens as outer membrane O-type polysaccharides independent from the smooth lipopolysaccharide. *J. Bacteriol.* **178**, 1070–1079
  20. Galanos, C., Lüderitz, O., and Westphal, O. (1969) A new method for the extraction of R-lipopolysaccharides. *Eur. J. Biochem.* **9**, 245–249
  21. Velasco, J., Bengoechea, J. A., Brandenburg, K., Lindner, B., Seydel, U., González, D., Zähringer, U., Moreno, E., and Moriyón, I. (2000) *Brucella abortus* and its closest phylogenetic relative, *Ochrobactrum* spp., differ in outer membrane permeability and cationic peptide resistance. *Infect. Immun.* **68**, 3210–3218
  22. Posch, G., Andrukhov, O., Vinogradov, E., Lindner, B., Messner, P., Holst, O., and Schäffer, C. (2013) Structure and immunogenicity of the rough-type lipopolysaccharide from the periodontal pathogen *Tannerella forsythia*. *Clin. Vaccine Immunol.* **20**, 945–953
  23. Holst, O., Thomas-Oates, J. E., and Brade, H. (1994) Preparation and structural analysis of oligosaccharide monophosphates obtained from the lipopolysaccharide of recombinant strains of *Salmonella minnesota* and *Escherichia coli* expressing the genus-specific epitope of *Chlamydia lipopolysaccharide*. *Eur. J. Biochem.* **222**, 183–194
  24. Wu, D., Chen, A., and Johnson, C. S. (1995) An improved diffusion-ordered spectroscopy experiment incorporating bipolar-gradient pulses. *J. Magn. Reson. Ser. A* **115**, 260–264
  25. Bax, A., and Davis, D. G. (1985) MLEV-17-based two-dimensional homonuclear magnetization transfer spectroscopy. *J. Magn. Reson.* **65**, 355–360
  26. Schleucher, J., Schwendinger, M., Sattler, M., Schmidt, P., Schedletzky, O., Glaser, S. J., Sørensen, O. W., and Griesinger, C. (1994) A general enhancement scheme in heteronuclear multidimensional NMR employing pulsed field gradients. *J. Biomol. NMR* **4**, 301–306
  27. Tannús, A., and Garwood, M. (1997) Adiabatic pulses. *NMR Biomed.* **10**, 423–434
  28. Kupč, Ě. (2001) Applications of adiabatic pulses in biomolecular nuclear magnetic resonance. *Methods Enzymol.* **338**, 82–111
  29. Böhlen, J.-M., and Bodenhausen, G. (1993) Experimental aspects of Chirp NMR spectroscopy. *J. Magn. Reson. Ser. A* **102**, 293–301
  30. Nyberg, N. T., Duus, J. Ø., and Sørensen, O. W. (2005) Heteronuclear two-bond correlation: suppressing heteronuclear three-bond or higher NMR correlations while enhancing two-bond correlations even for vanishing  ${}^2J_{\text{CH}}$ . *J. Am. Chem. Soc.* **127**, 6154–6155
  31. Kumar, A., Ernst, R. R., and Wüthrich, K. (1980) A two-dimensional nuclear Overhauser enhancement (2D NOE) experiment for the elucidation of complete proton-proton cross-relaxation networks in biological macromolecules. *Biochem. Biophys. Res. Commun.* **95**, 1–6
  32. Bax, A., and Summers, M. F. (1986)  ${}^1\text{H}$  and  ${}^{13}\text{C}$  assignments from sensitivity-enhanced detection of heteronuclear multiple-bond connectivity by 2D multiple quantum NMR. *J. Am. Chem. Soc.* **108**, 2093–2094
  33. Claridge, T. D., and Pérez-Victoria, I. (2003) Enhanced  ${}^{13}\text{C}$  resolution in semi-selective HMBC: a band-selective, constant-time HMBC for complex structure elucidation by NMR. *Org. Biomol. Chem.* **1**, 3632–3634
  34. Zartler, E. R., and Martin, G. E. (2011) The use of  ${}^1\text{H}$ - ${}^{31}\text{P}$  GHMBC and covariance NMR to unambiguously determine phosphate ester linkages in complex polysaccharide mixtures. *J. Biomol. NMR* **51**, 357–367
  35. Kellogg, G. W. (1992) Proton-detected hetero TOCSY experiments with application to nucleic acids. *J. Magn. Reson.* **98**, 176–182
  36. Inaba, K., Inaba, M., Romani, N., Aya, H., Deguchi, M., Ikehara, S., Muramatsu, S., and Steinman, R. M. (1992) Generation of large numbers of dendritic cells from mouse bone marrow cultures supplemented with granulocyte/macrophage colony-stimulating factor. *J. Exp. Med.* **176**, 1693–1702
  37. Grilló, M.-J., Blasco, J. M., Gorvel, J. P., Moriyón, I., and Moreno, E. (2012) What have we learned from brucellosis in the mouse model? *Vet. Res.* **43**, 29
  38. Holst, O., Broer, W., Thomas-Oates, J. E., Mamat, U., and Brade, H. (1993) Structural analysis of two oligosaccharide bisphosphates isolated from the lipopolysaccharide of a recombinant strain of *Escherichia coli* F515 (Re chemotype) expressing the genus-specific epitope of *Chlamydia* lipopolysaccharide. *Eur. J. Biochem.* **214**, 703–710
  39. De Boer, W. R., Kruyssen, F. J., and Wouters, J. T. (1976) The structure of teichoic acid from *Bacillus subtilis* var. *niger* WM as determined by  ${}^{13}\text{C}$  nuclear-magnetic-resonance spectroscopy. *Eur. J. Biochem.* **62**, 1–6
  40. Holst, O., Röhrscheidt-Andrzejewski, E., and Brade, H. (1990) Isolation and characterisation of 3-deoxy-D-manno-2-octulopyranosonate 7-(2-aminoethyl phosphate) from the inner core region of *Escherichia coli* K-12 and *Salmonella minnesota* lipopolysaccharides. *Carbohydr. Res.* **204**, 93–102
  41. Mühlradt, P. F., Wray, V., and Lehmann, V. (1977) A  ${}^{31}\text{P}$  nuclear magnetic resonance study of the phosphate groups in lipopolysaccharide and lipid A from *Salmonella*. *Eur. J. Biochem.* **81**, 193–203
  42. Stewart, A., Bernlind, C., Martin, A., Oscarson, S., Richards, J. C., and Schweda, E. K. H. (1998) Studies of alkaline mediated phosphate migration in synthetic phosphoethanolamine L-glycero-D-manno-heptoside derivatives. *Carbohydr. Res.* **313**, 193–202
  43. Brabetz, W., Müller-Loennies, S., Holst, O., and Brade, H. (1997) Deletion of the heptosyltransferase genes *rfaC* and *rfaF* in *Escherichia coli* K-12 results in an Re-type lipopolysaccharide with a high degree of 2-aminoethanol phosphate substitution. *Eur. J. Biochem.* **247**, 716–724
  44. Qureshi, N., Takayama, K., Seydel, U., Wang, R., Cotter, R. J., Agrawal, P. K., Bush, C. A., Kurtz, R., and Berman, D. T. (1994) Structural analysis of the lipid A derived from the lipopolysaccharide of *Brucella abortus*. *J. Endotoxin Res.* **1**, 137–148
  45. Conde-Álvarez, R., Arce-Gorvel, V., Gil-Ramírez, Y., Iriarte, M., Grilló, M.-J., Gorvel, J. P., and Moriyón, I. (2013) Lipopolysaccharide as a target for brucellosis vaccine design. *Microb. Pathog.* **58**, 29–34
  46. Godfroid, F., Taminiau, B., Danese, I., Denoel, P., Tibor, A., Weynants, V., Cloeckert, A., Godfroid, J., and Letesson, J. J. (1998) Identification of the perosamine synthetase gene of *Brucella melitensis* 16M and involvement of lipopolysaccharide O side chain in *Brucella* Survival in Mice and in Macrophages. *Infect. Immun.* **66**, 5485–5493
  47. Zhao, G., Liu, J., Liu, X., Chen, M., Zhang, H., and Wang, P. G. (2007) Cloning and characterization of GDP-perosamine synthetase (Per) from *Escherichia coli* O157:H7 and synthesis of GDP-perosamine *in vitro*. *Biochem. Biophys. Res. Commun.* **363**, 525–530